Research Article
DILI, Autoimmune, Cholestatic and Genetic Diseases

JOURNAL
OF HEPATOLOGY

Claudin-1 is a mediator and therapeutic target in primary sclerosing cholangitis

Authors

Fabio Del Zompo, Emilie Crouchet, Tessa Ostyn, …, Olivier Govaere, Catherine Schuster, Thomas F. Baumert

Correspondence

thomas.baumert@unistra.fr (T.F. Baumert).

Graphical abstract

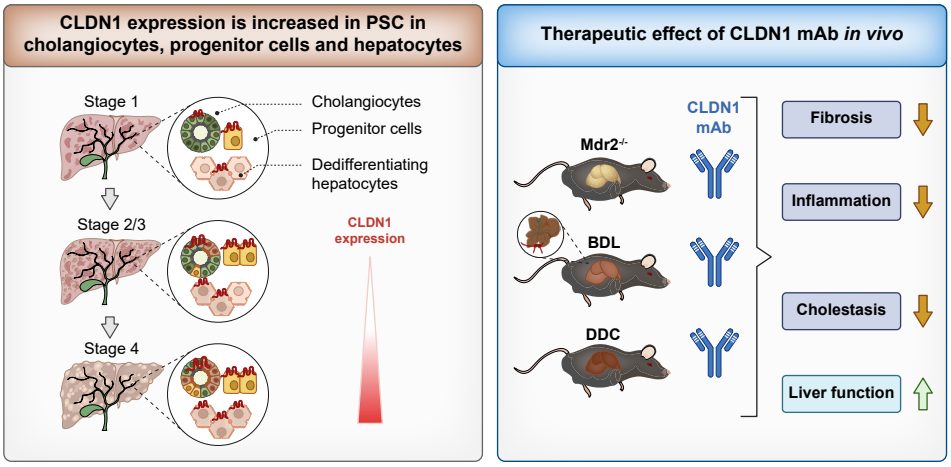

Highlights

- Claudin-1 is overexpressed in PSC cholangiocytes and its expression correlates with prognosis in patients.
- Spatial transcriptomics, proteomics, and loss-of-function studies unravel Claudin-1 as a disease driver.
- Treatment with a Claudin-1-specific monoclonal antibody improves survival, fibrosis, inflammation and cholestasis in PSC mouse models.
- Claudin-1 antibodies inhibit profibrotic and proinflammatory signaling in cholangiocytes.
- Preclinical proof-of-concept supports further development of Claudin-1-specific monoclonal antibodies for patients with PSC.

Impact and implications

Primary sclerosing cholangitis (PSC) is a chronic fibrosing cholangiopathy with limited therapeutic options. We identified the cell surface protein Claudin-1 as a key mediator and potential therapeutic target for PSC. In patients, Claudin-1 expression correlates with disease stage and clinical outcomes. Conditional liver epithelial-specific Claudin-1 knockout in mice reduced liver injury, fibrosis, and cholestasis. Monoclonal antibodies targeting Claudin-1 inhibited fibrosis, cholestasis, and the ductular reaction across advanced PSC mouse models by suppressing pro-inflammatory and fibrogenic signaling. These preclinical findings support the clinical development of Claudin-1-specific antibodies for PSC treatment and have significant implications for physicians, researchers, and drug developers in the field of biliary disease.

https://doi.org/10.1016/j.jhep.2025.08.005
 J. Hepatol. 2025, 83, 1305–1319

Research Article
DILI, Autoimmune, Cholestatic and Genetic Diseases

JOURNAL OF HEPATOLOGY

Claudin-1 is a mediator and therapeutic target in primary sclerosing cholangitis

Fabio Del Zompo[1], Emilie Crouchet[1], Tessa Ostyn[2], Zeina Nehme[1], Mélissa Messé[1], Frank Jühling[1], Romain Désert[1], Angelica T. Vieira[1], Julien Moehlin[1], Diana Nakib[3,4], Tallulah Andrews[3,4], Catia Perciani[3,4], Sai Chung[3,4], Gary D. Bader[5], Ian McGilvray[4], Chiara Caime[6,7], Miki Scaravaglio[6,7], Marco Carbone[7,8], Pietro Invernizzi[6,7], Sheraz Yaqub[9], Trine Folseraas[10], Tom H. Karlsen[10], Gautam Shankar[2,11], Mark Primeaux[12], Punita Dhawan[12], Jesus M. Banales[13,14], Natascha Roehlen[1,§], Roberto Iacone[15], Geoffrey Teixeira[15], Mathias Heikenwälder[16,17], Laurent Mailly[1], Sonya MacParland[3,4], Tania Roskams[2], Olivier Govaere[2], Catherine Schuster[1], Thomas F. Baumert[1,18,19,20,*]

Journal of Hepatology **2025**. vol. 83 | 1305–1319

Check for updates

Background & Aims: Primary sclerosing cholangitis (PSC) is a cholangiopathy associated with a high risk of progression to end-stage liver disease and hepatobiliary cancer. Its pathogenesis remains poorly understood, and current clinical management offers limited therapeutic options, primarily liver transplantation. Claudin-1 (CLDN1), a transmembrane protein highly expressed in liver epithelial cells, plays a critical role in cell-cell communication and signaling. We aimed to investigate the functional role of CLDN1 as both a mediator and potential therapeutic target for PSC using patient cohorts alongside murine and patient-derived intervention models.

Methods: CLDN1 expression patterns and associated cellular phenotypes were analyzed in liver tissues from five PSC patient cohorts using single-cell RNA sequencing, spatial transcriptomics, and multiplex proteomics. Proof-of-concept studies employing CLDN1-specific monoclonal antibodies (mAbs) and genetic loss-of-function approaches were performed in state-of-the-art mouse models of PSC and cholangiopathies. Perturbation studies in human cell-based models were conducted to explore underlying mechanisms.

Results: In liver tissues from patients with PSC, CLDN1 expression was markedly upregulated and correlated with disease progression. Spatial transcriptomics and proteomics revealed elevated CLDN1 expression in diseased cholangiocytes and cholestatic periportal hepatocytes, accompanied by activation of pro-inflammatory and pro-fibrotic signaling pathways. Therapeutic administration of CLDN1-specific mAbs or genetic knockout improved liver function in PSC mouse models by reducing hepatobiliary fibrosis and cholestasis. Mechanistic studies indicated that mAb treatment inhibited pro-inflammatory and pro-fibrotic signaling in cholangiocytes and hepatocytes perturbed in PSC liver tissues.

Conclusions: These findings demonstrate a functional role for CLDN1 in the pathogenesis of PSC and biliary fibrosis. *In vivo* proof-of-concept studies, combined with expression analyses in patients with PSC, support the clinical development of CLDN1-specific mAbs as a therapeutic strategy for PSC.

Introduction

Primary sclerosing cholangitis (PSC) is a progressive cholestatic liver disease of unknown origin. Genetic and autoimmune mechanisms have been suggested as predisposing factors, although the exact pathogenesis remains elusive.[1,2] The natural course of PSC leads to biliary fibrosis and strictures, resulting in chronic cholestasis and progressing to cirrhosis and liver failure. Liver cancer is a major complication of PSC at any stage. The risk of cholangiocellular carcinoma (CCA) is estimated at 20%.[3] Liver transplantation is the only therapeutic option available for patients with advanced disease, limited by recurrence in up to 25% of recipients.[3] Histological hallmarks of the disease are inflammation, fibrosis, cholestasis, and the ductular reaction, which is considered a mediator of disease progression.[4,5] While a large series of compounds have been investigated in clinical trials, none has been shown to alter the natural progression of PSC.[1,6,7] The

* Corresponding author. Address: Inserm U1110, ITM, University of Strasbourg, 3 Rue Koeberlé, 67000 Strasbourg, France, Tel.: (+33) 3365583703.
E-mail address: thomas.baumert@unistra.fr (T.F. Baumert).
§ Present address: Department of Medicine II, Gastroenterology, Hepatology, Endocrinology and Infectious Diseases, Freiburg University Medical Center, Faculty of Medicine, University of Freiburg, Freiburg, Germany; Berta-Ottenstein-Programme, Faculty of Medicine, University of Freiburg, Freiburg, Germany.
https://doi.org/10.1016/j.jhep.2025.08.005

lack of approved disease-modifying drugs shows the high unmet clinical need for new therapeutic strategies.

CLDN1 is a transmembrane protein highly expressed in epithelial cells mediating cell-cell communication and signaling.[8] CLDN1 has been shown to play a functional role in the disease biology of inflammation, fibrosis and cancer.[8–11] In the liver, it is expressed in both junctional and non-junctional forms, exposed on the basolateral membrane of polarized hepatocytes, where it contributes to liver fibrosis and progression to hepatocellular carcinoma (HCC).[8,9,12] We have previously developed monoclonal antibodies (mAbs) targeting a conformational epitope in the CLDN1 extracellular loop 1 comprising motif W(30)-GLW(51)-C(54)-C(64). The mAbs are highly specific for non-junctional CLDN1 without cross-reactivity to other Claudins.[13] In a metabolic dysfunction-associated steatohepatitis (MASH)-driven HCC mouse model, mAb treatment inhibited liver fibrosis and progression to HCC, showing an excellent safety profile in non-human primates and healthy volunteers.[8,12,14] While patients with genetic CLDN1 mutations can present with sclerosing cholangitis,[15] the functional role of CLDN1 in PSC disease biology is unknown. Here, we investigated the functional role of CLDN1 as a mediator and therapeutic target in PSC.

Materials and methods

Patient selection

CLDN1 expression was investigated in five cohorts of patients with cholangiopathies. Liver transcriptomic datasets of patients with PSC and their respective controls were retrieved from ArrayExpress (EMBL-EBI), accession number E-GEOD-61260[16], and Gene Expression Omnibus (NIH), accession numbers GSE118373,[4] GSE243981.[17] FFPE liver samples of patients with PSC were retrospectively obtained from the biobanks of the Norwegian PSC Research Center of Oslo, Norway (Table S1), the Department of Medicine and Surgery of

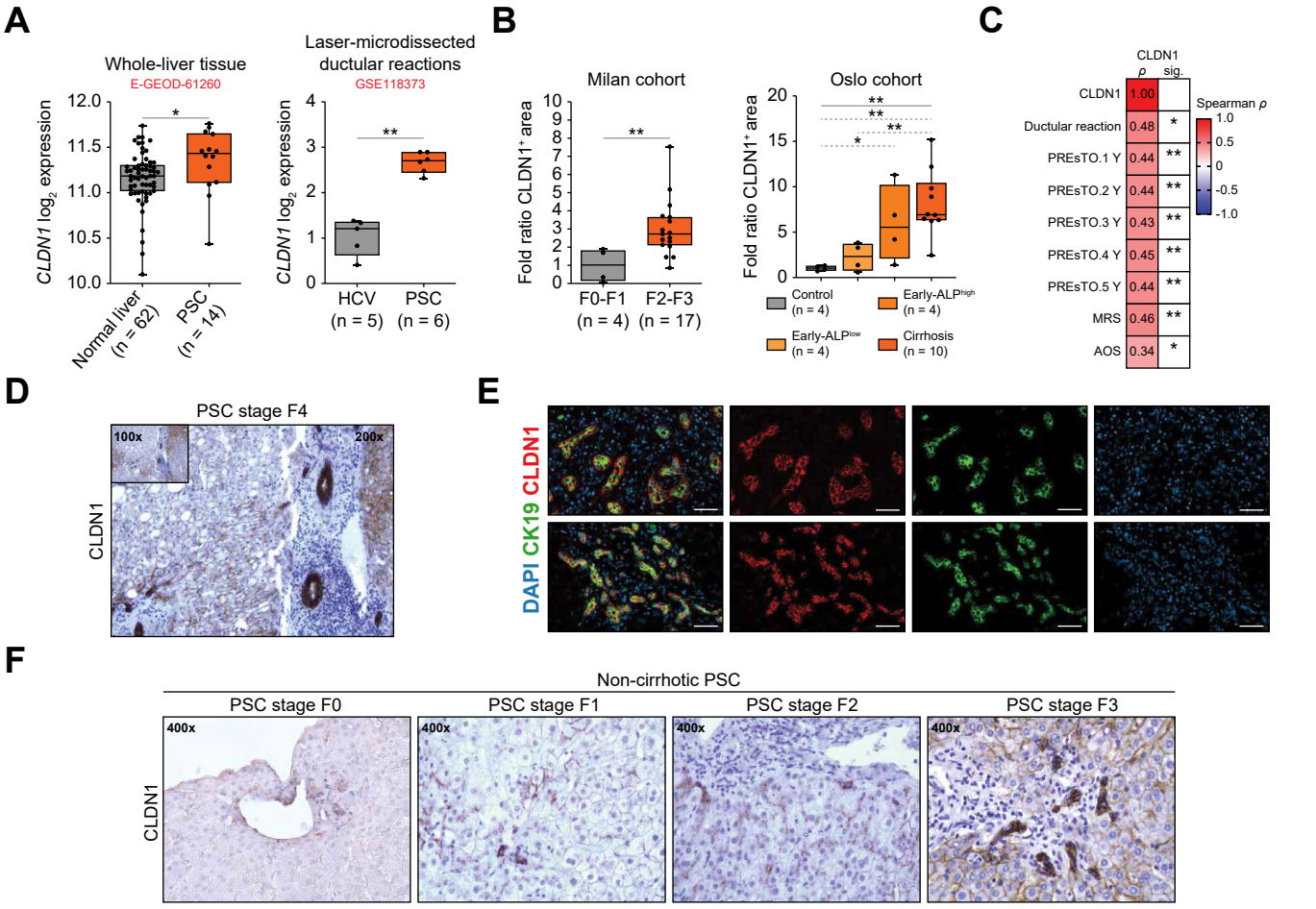

Fig. 1. CLDN1 is upregulated in liver tissues from patients with PSC and correlates with disease progression. (A) *CLDN1* gene expression in whole-liver tissues (Mann-Whitney, $p = 0.0175$)(E-GEOD-61260)[16] and laser micro-dissected ductular reaction areas of patients with PSC (Mann-Whitney, $p = 0.0043$)(GSE118373).[4] (B) Quantification of CLDN1 expression in CLDN1-stained liver biopsies from two independent cohorts of patients with PSC, showing marked CLDN1 upregulation in patients, associated with fibrosis stage (Milan cohort: Mann-Whitney, $p = 0.009$; Oslo cohort, continuous line indicates Kruskal-Wallis $p = 0.0036$; dashed lines indicate pairwise Mann-Whitney: control *vs.* Early-ALP^{high} $p = 0.0286$; control *vs.* cirrhosis $p = 0.002$; Early-ALP^{low} *vs.* cirrhosis $p = 0.008$. (C) CLDN1 protein expression correlates with clinical prognostic scores, including the magnitude of the ductular reaction (Spearman's correlation, $p = 0.019$, $p = 0.004$, $p = 0.004$, $p = 0.004$, $p = 0.004$, $p = 0.004$, $p = 0.04$, $p = 0.04$ top to bottom). (D) Immunohistochemical staining on a PSC liver explant reveals strong CLDN1 expression in damaged bile ducts, ductular reaction, and cholestatic peri-portal hepatocytes. (E) Immunofluorescent staining showing robust CLDN1 expression in CK19-positive cells in PSC samples. Scale bars: 50 μm. (F) CLDN1 IHC staining of PSC samples at different stages, showing CLDN1 expression increasing along with disease stage, ductular reaction, and fibrotic content. * p <0.05; ** p <0.01; *** p <0.001; **** p <0.0001. ALP, alkaline phosphatase; CK19, cytokeratin 19; CLDN1, Claudin-1; IHC, immunohistochemistry; PSC, primary sclerosing cholangitis. (This figure appears in color on the web.)

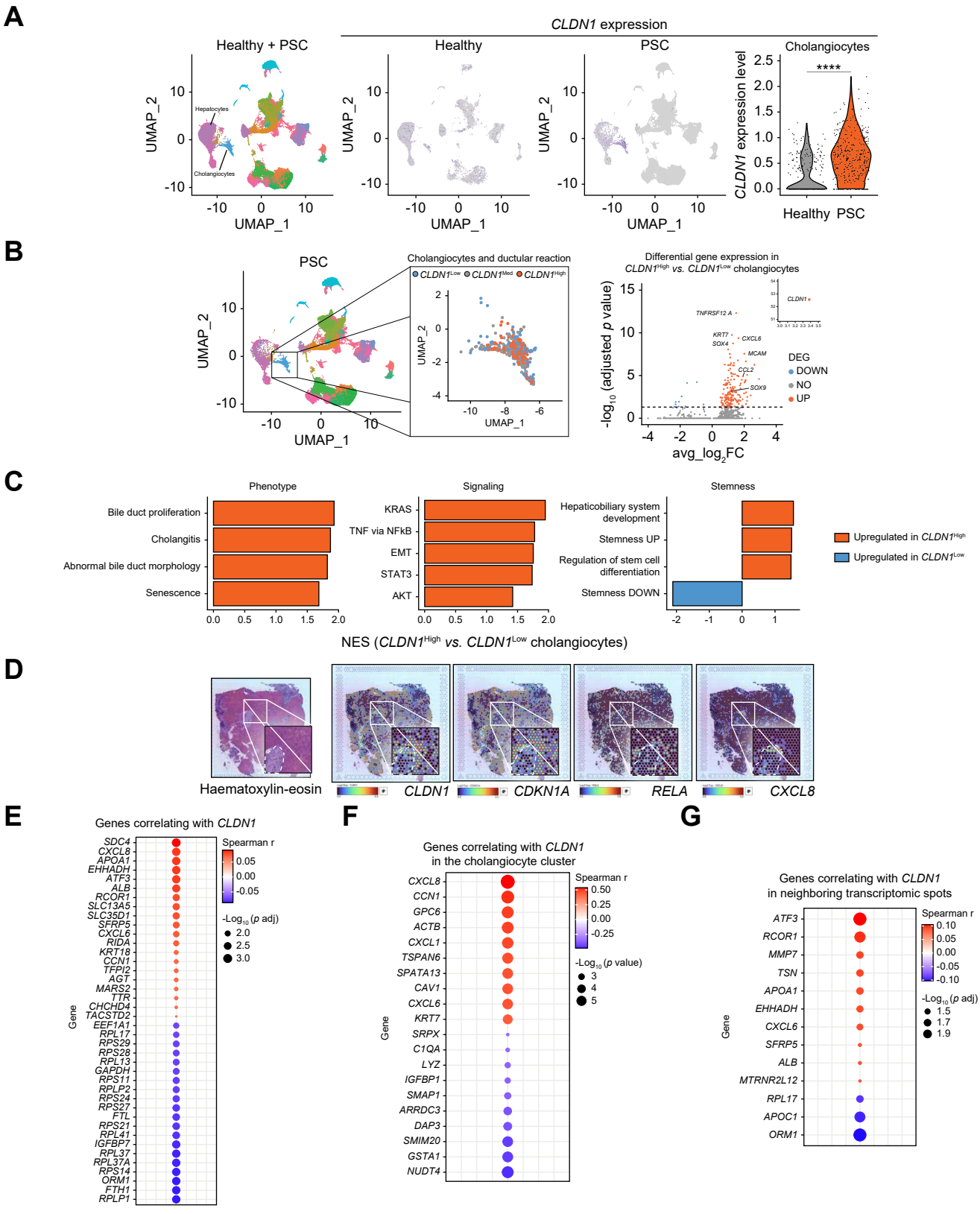

Fig. 2. CLDN1 expression co-localizes with known PSC disease drivers in patients. (A) In a published PSC scRNA-seq atlas,[17] *CLDN1* is upregulated in cholangiocytes of patients with PSC. (B) DEG analysis in PSC-derived *CLDN1*^{High} *vs.* *CLDN1*^{Low} biliary epithelial cells. Analysis of a spatial transcriptomic atlas of PSC.[17] (C) Pathway enrichment analyses revealed that *CLDN1*^{High} biliary cells are characterized by distinct signaling, phenotype, and plasticity features compared to *CLDN1*^{Low} counterparts. (D) Analysis of a spatial transcriptomic atlas of PSC.[18] *CLDN1* expression co-localizing with *CDKN1A*, *RELA*, and *CXCL8* at the interface of scar lesions. Insets show the interface region between a peribiliary scar and surrounding non-fibrotic liver tissue. Dashed lines delineate a fibrotic scar. (E) Whole PSC liver unbiased analysis of top 40 genes significantly correlating with *CLDN1* expression. (F) Top 20 genes significantly correlating with *CLDN1* expression in the 'Cholangiocyte' cluster. (G) Genes significantly correlating with *CLDN1* expression in a neighboring transcriptomic spot. CLDN1, Claudin-1; DEG, differentially expressed gene; PSC, primary sclerosing cholangitis; scRNA-seq, single-cell RNA sequencing. (This figure appears in color on the web.)

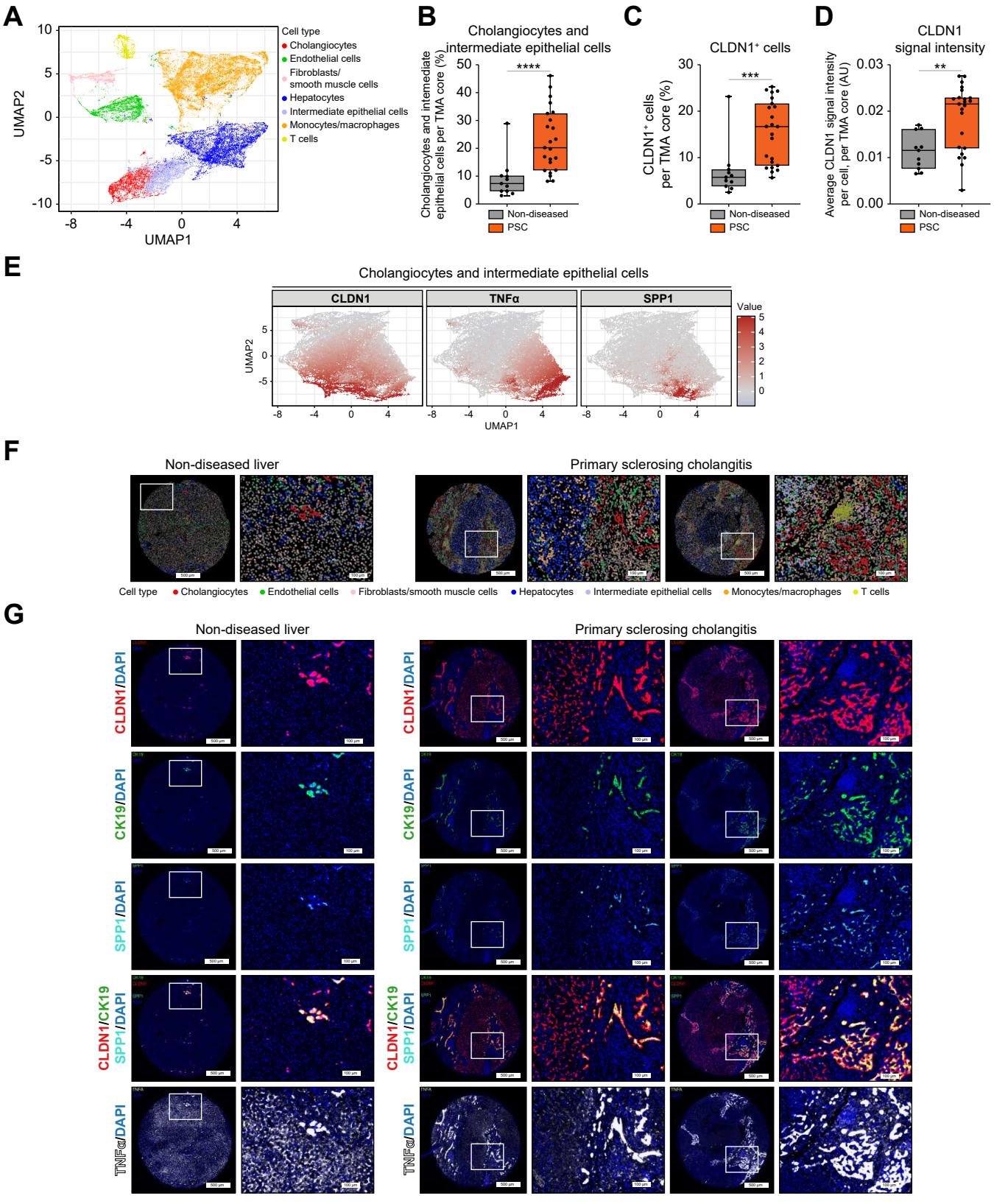

Fig. 3. Spatial multiplex proteomics reveals an increase in CLDN1-expressing liver epithelial cells in PSC liver tissues at the single-cell level. (A) UMAP clustering of spatial proteomics-phenotyped liver tissue cells. (B) Quantitative cytometry shows increased numbers of cholangiocytes and intermediate epithelial cells in PSC compared to non-diseased livers (Mann-Whitney, p <0.0001). Expression of CK19+CK7+ was used to identify cholangiocytes including ductular reactive cells, staining of CK18+CK7+CK19- cells were used to identify intermediate epithelial cells, such as dedifferentiating hepatocytes. (C) Quantitative cytometry shows

the University of Milano-Bicocca, Italy (Table S2), and the University Hospital Leuven, Belgium (Table S3). Biopsies were assessed by an expert liver pathologist. The use of human samples was approved by the respective local ethical committees with informed patient consent.

Computational analyses of patient samples

Raw count matrices from microarray studies were pre-processed and normalized using the *oligo* package in R. Single-cell RNA sequencing (scRNA-seq) PSC expression data[17] were analyzed using *Seurat*, *rstatix*, and *fgsea* packages in R. PSC spatial transcriptomics dataset[17] was analyzed using *Seurat* package in R. Detailed technical information is described in the supplementary material and methods.

Immunohistochemistry, immunofluorescence, and multiple iterative labelling by antibody neodeposition

Detailed technical information is described in the supplementary material and methods.

Antibodies

Monoclonal anti-CLDN1 and IgG isotype control antibodies have been described.[8,18] Staining antibodies are described in Tables S5–S6.

Animal experiments

The bile duct ligation (BDL), 3,5-diethoxycarbonyl-1,4-dihydrocollidine (DDC) and *Mdr2*$^{-/-}$ mouse models,[19] expressing a human/mouse chimeric CLDN1 as a knock-in, were used to study the efficacy and safety of CLDN1 mAbs *in vivo*. Details are described in the supplementary materials and methods.

Bioinformatic and statistical analyses

Bioinformatic procedures are described in supplementary data. Continuous data were compared using Student's *t* test when normally distributed (Shapiro-Wilk test) or non-parametric tests (Mann-Whitney *U* test and Kruskal-Wallis test) when non-normally distributed. Correlation was assessed by Spearman correlation test. Categorical data were analyzed using Fisher's exact test. Outlier identification was carried out using the ROUT method (Q = 1%). p values <0.05 were considered statistically significant. Statistical analyses were performed using GraphPad Prism 9 and R.

Results

Claudin-1 expression is upregulated in the livers of patients with PSC and correlates with disease progression

To investigate the role of CLDN1 in clinical disease biology, CLDN1 expression was analyzed in PSC cohorts by immunohistochemistry (IHC) and quantitative proteomics at the single-cell level. Furthermore, publicly available single-cell,[17] spatial,[17] and bulk RNA transcriptomic[4,16] data sets of patients with PSC were analyzed (Figs 1-3).

CLDN1 gene expression was markedly and significantly upregulated in liver tissues of patients with PSC, including the pro-fibrogenic ductular reaction (Fig. 1A). IHC staining of PSC samples from two well characterized cohorts (Milan, Oslo, Tables S1–2) revealed that CLDN1 protein upregulation was robustly associated with disease progression (Fig. 1B, Tables S1–2), as shown by markedly increased CLDN1 expression with progressing liver fibrosis stage (Fig. 1B), independent of comorbid inflammatory bowel disease (IBD) (Fig. S1A). CLDN1 expression in patient liver tissues correlated with clinically validated prognostic scores including the Amsterdam-Oxford PSC score, the Mayo risk score for PSC, and the PREsTO score[20,21](Fig. 1C and S1B). CLDN1 expression also correlated with the magnitude of the ductular reaction (Fig. 1C), which is associated with poor prognosis in PSC.[5] Immunohistopathology analyses revealed that CLDN1 is robustly expressed in cholangiocytes lining damaged bile ducts, as well as ductular reactive cells (Fig. 1D). Hepatocytes close to portal spaces showed elevated CLDN1 expression with a membranous pattern, likely in association with a cholestatic metaplastic phenotype (Fig. 1D). Multi-color fluorescent staining validated high CLDN1 protein expression in virtually all cytokeratin (CK) 19+ ductular cells in PSC liver tissues (Fig. 1E). Consistently, CLDN1 protein expression increased with disease progression from early to advanced fibrosis stages in non-cirrhotic PSC liver samples, along with ductular reactive cells and liver fibrotic content in immunohistochemistry analyses (Fig. 1F).

The marked upregulation of CLDN1 in PSC tissues, its expression in PSC-driving cells, and its association with disease progression suggest that CLDN1 plays a pathogenic role in PSC and represents a potential therapeutic target.

Spatial transcriptomics and multi-plex proteomics in PSC liver tissues reveals co-localization of CLDN1 with known drivers of inflammation, fibrogenesis and stemness

To investigate the biological role of CLDN1 in PSC progression, its expression in liver samples of PSC was investigated by single cell-resolved and spatial transcriptomics. At the single-cell level, the highest *CLDN1* expression levels were found in cells expressing markers of the biliary lineage, including cholangiocytes and biliary epithelial cells (Fig. 2A). An unbiased analysis of marker genes in CLDN1^{High} cholangiocytes (Fig. 2B) revealed that top four differentially expressed genes included TNF-related weak inducer of apoptosis receptor (TWEAK receptor, *TNFRSF12A*), cytokeratin 7 (*KRT7*), chemokine (C-X-C motif) ligand 6 (*CXCL6*), and SRY-box transcription factor 4 (*SOX4*) (Fig. 2B and S2A). Confirmatory studies at the protein level revealed that CLDN1+ CK19+ biliary epithelial cells were the major source of TNFα in PSC liver tissues (Fig. S2B). Gene set-enrichment analysis of

increased numbers of CLDN1+ cells in PSC compared to non-diseased livers (Mann-Whitney, p = 0.0002). (D) Quantitative cytometry showing increased CLDN1 staining intensity in CLDN1+ cells in PSC compared to non-diseased livers (Mann-Whitney, p = 0.0034). (E) Protein expression of CLDN1, TNFα, and SPP1/osteopontin in the cluster of cholangiocytes and intermediate epithelial cells. (F) Digital reconstruction of representative TMA cores, phenotyped by spatial proteomics. (G) Individual panels showing representative TMA cores stained for CLDN1, CK19, SPP1, CLDN1+CK19+SPP1, and TNFα (upper to lower). ***p <0.001; ****p <0.0001. CLDN1, Claudin-1; PSC, primary sclerosing cholangitis; TMA, tissue microarray; UMAP, uniform manifold approximation and projection. (This figure appears in color on the web.)

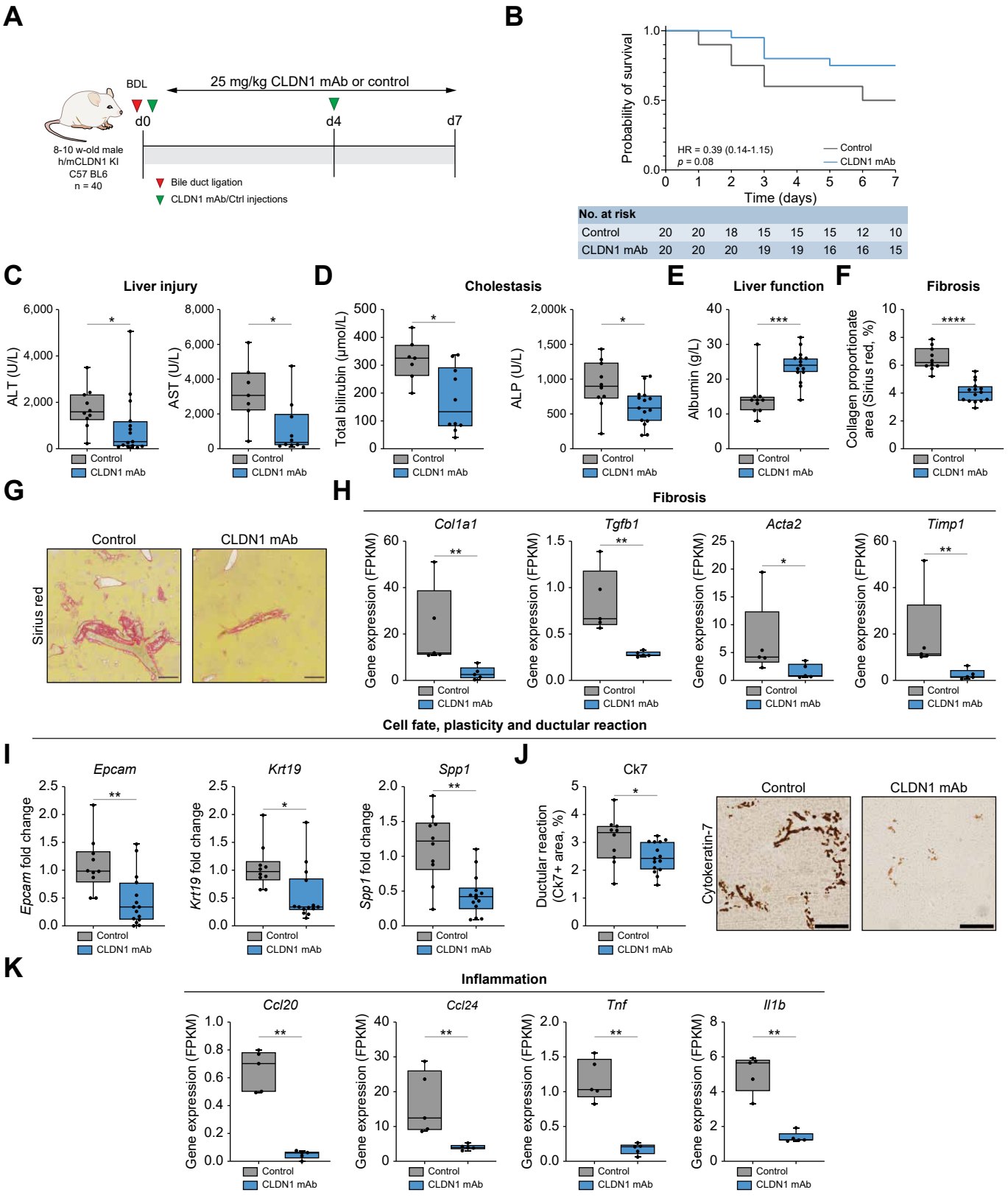

Fig. 4. CLDN1 mAb treatment improves survival, liver function, cholestasis, and liver fibrosis in the bile duct ligation mouse model. (A) Illustration of the experimental approach. (B) Survival analysis of bile duct-ligated mice revealed that CLDN1 mAb improved survival at 7 days (Log-rank test, $p = 0.08$). (C-E) CLDN1 mAb treatment significantly ameliorated liver function tests, included ALT (Mann-Whitney, $p = 0.0163$) and AST (Mann-Whitney, $p = 0.0185$) (C), total bilirubin (Mann-Whitney, $p = 0.0118$) and ALP (Mann-Whitney, $p = 0.0168$) as markers of cholestasis (D), and albumin (Mann-Whitney, $p = 0.0006$) as a marker of liver biosynthetic function (E). (F) CLDN1 mAb treatment reduced fibrosis levels as measured by Sirius red CPA (Mann-Whitney, $p < 0.0001$). (G) Representative images of Sirius red-

CLDN1^{High} *vs*. CLDN1^{Low} differentially expressed genes revealed that high CLDN1 expression was associated with gene sets of bile duct proliferation, cholangitis, and senescence (Fig. 2C, left). Signaling pathways associated with CLDN1 expression included KRAS, NF-κB, epithelial-to-mesenchymal transition, STAT3, and AKT (Fig. 2C, middle). Additionally, stemness-related gene sets were enriched in CLDN1^{high} cholangiocytes (Fig. 2C, right). Analysis of a published spatial transcriptomics dataset[17] revealed that *CLDN1* gene expression co-localized with the expression of known drivers of PSC, including *CDKN1A* (p21), NF-κB effector *RELA* (p65), and *CXCL8* (IL-8), at the edges of PSC scar lesions (Fig. 2D). Interestingly, *CLDN1* expression correlated with the expression of pro-inflammatory and pro-fibrogenic genes, including *CXCL8* (Fig. 2E,F and S2C,D) and *CXCL6* and *MMP7* in transcriptomic regions neighboring high *CLDN1* expression (Fig. 2G and S2E). These findings suggest that high *CLDN1* expression is associated with expression of pro-inflammatory and pro-fibrogenic pathways.

To validate the key single-cell gene expression findings at the protein level, 291,283 cells were phenotyped across samples of an independent cohort of patients with PSC (Fig. 3A, Table S3) using multiplex spatial proteomic analysis based on multiple iterative labelling by antibody neodeposition.[22] Quantitative cytometry in PSC *vs*. non-diseased tissues revealed a marked increase of CK19+CK7+ cholangiocytes including ductular reactive cells and CK18+CK7+CK19- intermediate epithelial cells, such as dedifferentiating hepatocytes (Fig. 3B). A robust and significant increase of the total number of CLDN1+ cells in PSC compared to non-diseased liver tissues was observed (Fig. 3C), along with the increase of CLDN1 signal intensity per cell (Fig. 3D), validating the results obtained by IHC (Figs 1 and 2) at single-cell resolution in an independent cohort. Protein expression analysis indicated co-localization of CLDN1 with mediators of biliary inflammation and fibrosis, such as the pro-inflammatory cytokine TNFα, and immune and fibrosis modulator secreted phosphoprotein 1 (SPP1, osteopontin) in cholangiocytes and intermediate epithelial cells (Fig. 3E). CLDN1+TNFα+SPP1+ cells were observed surrounding peribiliary fibrotic lesions (Fig. 3F,G and S3A,B), suggesting a potential role for CLDN1 in the biology of diseased cholangiocytes.

Treatment with CLDN1-specific mAbs improves liver function and survival by reducing fibrosis and cholestasis in state-of-the-art mouse models of PSC

To study the functional role of CLDN1 in the disease biology of PSC and to investigate the role of CLDN1 as a therapeutic target, proof-of-concept studies were performed in three complementary PSC animal models using highly specific CLDN1-specific antibodies.

Since the mAbs partially cross-react with mouse CLDN1,[8] we engineered a mouse model expressing a human/mouse (h/m) hybrid CLDN1 in all organs and cells where native CLDN1 is expressed. This was achieved by exchanging three amino acids in the mouse CLDN1 EL1-coding region using homologous recombination. The BDL model was applied first as it recapitulates cholestasis-driven fibrosis, as well as cholangiocyte reactivity and ductular reaction.[19,23] Forty 8-10 week-old male mice underwent surgical ligation of the common bile duct. Mice received 25 mg/kg CLDN1 mAb (n = 20) or vehicle control (n = 20) i.p. immediately after surgery and again on day 4 (Fig. 4A). Survival analysis of BDL mice showed that CLDN1 mAb treatment improved survival at day 7 (Fig. 4B). Liver function tests revealed an improvement of markers of liver injury, liver function, and cholestasis in CLDN1 mAb-*vs.* control-treated mice as shown by reduced levels of alanine aminotransferase (ALT), aspartate aminotransferase (AST) (Fig. 4C), total bilirubin and alkaline phosphatase (ALP) (Fig. 4D). Bile acids remained unchanged (Fig. S4A). Furthermore, significantly increased levels of albumin (Fig. 4E) indicated liver function improvement. Automated analysis of the collagen proportionate area (CPA) (Fig. 4F,G and S4B) of Sirius red-stained livers revealed a significant reduction of liver fibrosis in CLDN1 mAb-*vs.* control-treated mice. Transcriptomic analyses revealed that CLDN1 mAb treatment modulated gene expression of fibrosis-related markers *Col1a1*, *Tgfb1, Acta2*, and *Timp1* in both RNA-seq (Fig. 4H) and qPCR (Fig. S4C) analyses. Moreover, a robust reduction of the expression of markers of the ductular reaction including *Epcam*, *Krt19*, *Spp1* (Fig. 4I) and cytokeratin-7 (Fig. 4J) was observed. Additionally, CLDN1 mAb-treated mice exhibited reduced expression of pro-inflammatory cytokines (Fig. 4K).

Next, the DDC mouse model was applied, a chemical model for PSC recapitulating key features of sclerosing cholangitis and peribiliary fibrosis.[24] Forty 8-week-old male mice were fed with a 0.1% DDC-supplemented diet for 4 weeks. Following establishment of peribiliary fibrosis in week 1,[24] mice were assigned 1:1 to receive weekly i.p. injections of 25 mg/kg CLDN1 mAb or vehicle control for 3 weeks (Fig. 5A). CLDN1 mAb treatment did not change survival (Fig. S5A) and decreased liver-to-body weight ratio (Fig. 5B). Analysis of liver function tests revealed significant decreases of plasma ALT (Fig. 5C) and bile acids (Fig. 5D), but not ALP (Fig. S5B). Treatment with CLDN1 mAb resulted in a significant and robust reduction of liver fibrosis as shown by CPA analysis (Fig. 5E). CLDN1 treatment also resulted in inhibition of porto-portal bridging fibrosis – a key marker of disease progression in patients (Fig. 5F and S5C). The decreased expression of cytokeratin-19 (*Krt19*) and cytokeratin-7 indicated that CLDN1 mAb treatment reduced the ductular reaction (Fig. 5G). Analysis of differentially expressed genes by RNA-seq and qPCR (Fig. S5D) revealed the downregulation of several pro-inflammatory mediators in CLDN1 mAb-treated mice (Fig. 5H

stained livers of control and CLDN1 mAb-treated mice. Scale bars: 500 μM. (H–K) Expression of fibrosis (H), cell fate and ductular reaction (I-J) and inflammation (K) markers in the livers of control and CLDN1 mAb-treated mice (*Col1a1*: $p = 0.0079$; *Tgfb1*: $p = 0.0079$; *Acta2*: $p = 0.0317$; *Timp1*: $p = 0.0079$, *Krt19*: $p = 0.0056$; *Spp1*: $p = 0.0011$; Ck7: $p = 0.0357$; *Ccl24*: $p = 0.0079$; *Tnf*: $p = 0.0079$; *Il1b*: $p = 0.0079$; Mann-Whitney). Scale bars: 250 μM *p <0.05; **p <0.01; ***p <0.001; ****p <0.0001. AST (C, right) and bilirubin (D, left) panels show n = 7 control and n = 10 CLDN1 mAb-treated mice. The plasma of eight control and five treated mice could not be analyzed due to hemolysis interfering with analyte measurements. Data in (H) and (K) were obtained from RNA-seq analyses of a subset of five representative liver tissues (n = 5 *vs.* n = 5). ALP, alkaline phosphatase; ALT, alanine aminotransferase; AST, aspartate aminotransferase; CLDN1, Claudin-1; CPA, collagen proportionate area; mAb, monoclonal antibody; PSC, primary sclerosing cholangitis. (This figure appears in color on the web.)

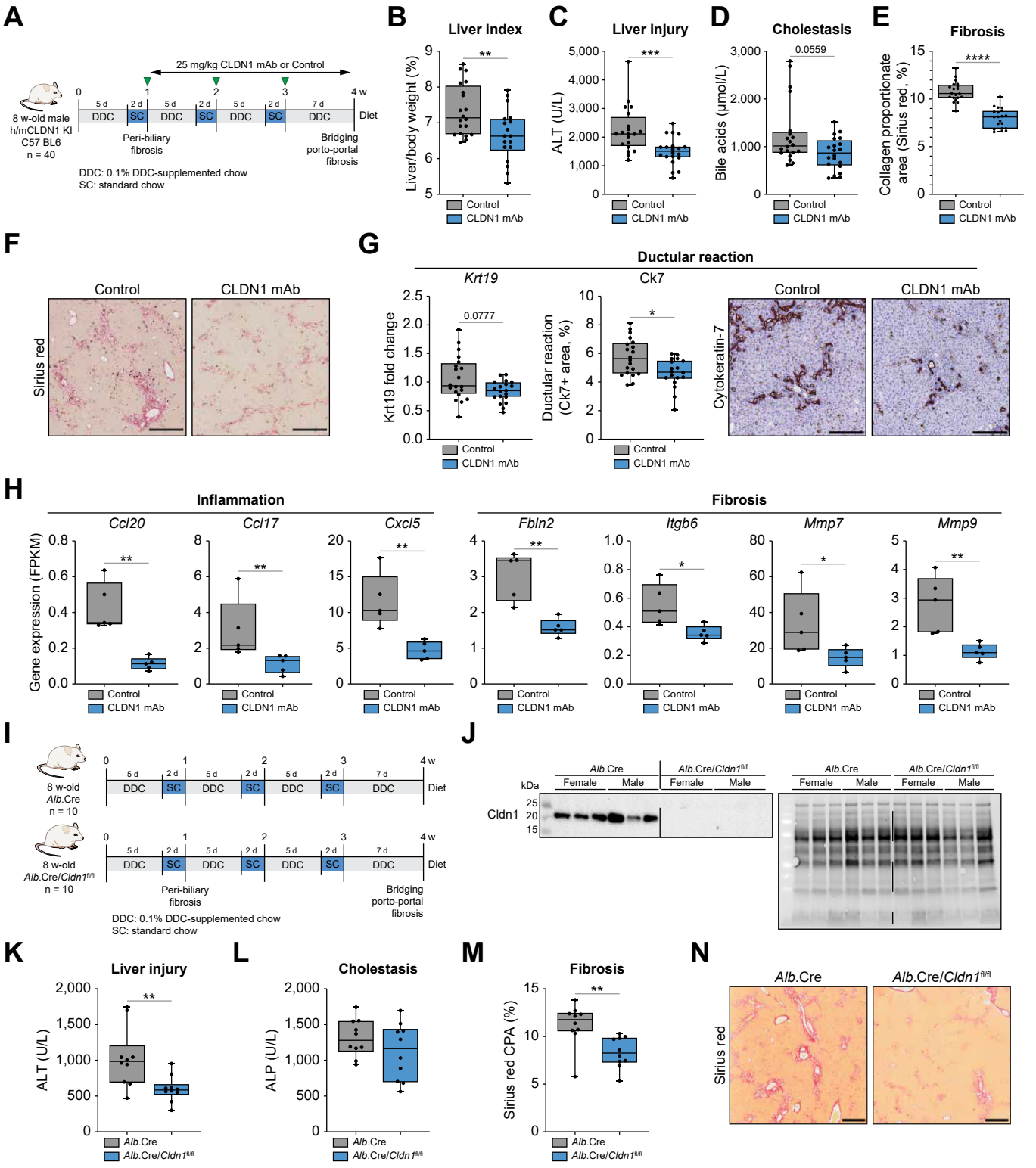

Fig. 5. CLDN1 mAb treatment ameliorates liver injury and fibrosis in the DDC mouse model. (A) Illustration of the experimental approach. (B) Analysis of the liver index (liver-to-body weight ratio) suggesting reduced cell proliferation in treated mice (Mann-Whitney, $p = 0.0055$). (C) CLDN1 mAb treatment ameliorated liver injury as shown by decreased levels of ALT (Mann-Whitney, $p = 0.0009$). (D) CLDN1 mAb treatment reduced cholestasis as measured by plasma concentrations of bile acids (Mann-Whitney, $p = 0.0559$). (E) CLDN1 mAb treatment reduced fibrosis levels as measured by Sirius red CPA (Mann-Whitney, $p < 0.0001$). (F) Representative images of Sirius red-stained livers of control and CLDN1 mAb-treated mice. Scale bars: 500 μM. (G) CLDN1 mAb treatment reduced the magnitude of ductular reaction, as measured by *Krt19* gene expression (Mann-Whitney, $p = 0.0777$) and cytokeratin-7 immunostaining (Mann-Whitney, $p = 0.0159$). Scale bars: 250 μM. (H) Liver expression (RNA-seq analyses of five liver tissues of each group, n = 5 *vs.* n = 5) of genes encoding for inflammation and fibrosis markers (*Ccl20*: $p = 0.0079$; *Ccl17* $p = 0.0079$; *Cxcl5*: $p = 0.0079$; *Fbln2*: $p = 0.0079$, *Itgb6*: $p = 0.0159$; *Mmp7*: $p = 0.0317$; *Mmp9*: $p = 0.0079$; Mann-Whitney). (I) Experimental approach of *Alb*.Cre/*Cldn1*$^{fl/fl}$ mice with conditional *Cldn1* knockout in liver epithelial cells and subjected to DDC diet. (J) Liver Cldn1 expression in *Alb*.Cre and *Alb*.Cre/*Cldn1*$^{fl/fl}$ mice,

and S5D). Confirming the histopathology findings, expression of genes involved in fibrogenesis and extracellular matrix remodeling was significantly decreased, including fibulin 2 (*Fbln2*), integrin subunit beta 6 (*Itgb6*), matrix metallopeptidase 7 (*Mmp7*), matrix metallopeptidase 9 (*Mmp9*)(Fig. 5H), and transforming growth factor beta 2 (*Tgfb2*)(Fig. S5D).

Since CLDN1 has been shown to be upregulated in the colon of patients with IBD,[25] the effect of CLDN1 mAb treatment on the colon was investigated. MAb treatment did not result in significant differences in colon length, colon weight, and intestinal permeability (Fig. S6A–E). Furthermore, no colon histopathological changes were observed, as previously shown for healthy mice across organs.[14] Treatment effects were similar in male and female mice (Figs S6B and S7A-C), suggesting that there is likely no sex-dependency for CLDN1 mAb efficacy. A control group fed standard chow served as a baseline to distinguish the specific effects of diet from other variables (Fig. S7A–D). The effects of CLDN1 mAb were target-specific, since an isotype control did not show therapeutic effects (Fig. S7A–D). Moreover, CLDN1 mAb treatment did not modulate liver function tests in h/mCLDN1 KI mice under non-disease modeling conditions (Fig. S7D).

To further validate the functional role of CLDN1 in the pathogenesis of biliary fibrosis, the generation of an *Alb*.Cre/*Cldn1*$^{fl/fl}$ mouse model enabled investigation of biliary fibrosis development in mice with *Cldn1* conditional knockout in liver epithelial cells. When challenged with 0.1% DDC feeding (Fig. 5I), *Alb*.Cre/*Cldn1*$^{fl/fl}$ robustly maintained the *Cldn1* knockout phenotype, as shown by the absence of CLDN1 expression in the liver (Fig. 5J), while exhibiting significantly less liver injury (Fig. 5K), less cholestasis (Fig. 5L), and less collagen deposition (Fig. 5M,N) compared to *Alb*.Cre controls.

The *Mdr2*$^{-/-}$ mouse model is a state-of-the-art model for PSC, as it recapitulates chronic disease progression, modeling biliary fibrosis, cholestasis and hepatobiliary cancer, similar to the clinical course of PSC.[26] *Mdr2*$^{-/-}$ mice were treated with CLDN1 mAb or control at the age of 6 weeks, when fibrosis and portal PSC-like lesions were already established.[26] After 12 weeks of treatment, mice were sacrificed, and plasma and livers harvested (Fig. 6A). While this model is characterized by low mortality, our data indicate that treatment with CLDN1 mAb improved survival compared to control animals (Fig. 6B). In a per-protocol analysis of relative weight change, CLDN1 mAb treatment significantly increased growth rate (Fig. 6C). CLDN1 mAb-treated *Mdr2*$^{-/-}$ mice exhibited a robust improvement of cholestasis as shown by reduced total bilirubin (Fig. 6D and S8A), plasma bile acids (Fig. 6D and S8B), and ALP (Fig. 6D). ALP levels, which are used as endpoints in clinical trials,[1] were normalized in 73% of CLDN1 mAb-treated mice *vs*. 28% of control-treated mice (Fig. 6D). The improvement of cholestasis was accompanied by reduced liver injury, as shown by decreased AST and ALT levels (Fig. 6E). Importantly, CLDN1 mAb treatment resulted in reduced liver fibrosis, including the inhibition of bridging fibrosis as shown by CPA analyses (Fig. 6F,G and S8C). The histopathological features of fibrosis reduction were accompanied by reduced gene expression of pro-inflammatory mediators (Fig. 6H). Analysis of cell fate marker expression revealed that CLDN1 mAb treatment downregulated biliary-fate marker *Sox9* while upregulating hepatic nuclear factor 4 alpha (*Hnf4a*) (Fig. 6I), while markers of the ductular reaction remained unchanged (Fig. S8D). The expression of extracellular matrix components collagen type IV alpha-1 chain (*Col4a1*), collagen type V alpha-2 chain (*Col5a2*), and laminin subunit beta 1 (*Lamb1*) was significantly downregulated in CLDN1 mAb-treated mice (Fig. 6J and S8E).

Collectively, proof-of-concept studies in three state-of-the-art PSC mouse models showed improvement of liver function, cholestasis, and fibrosis on CLDN1 mAb treatment.

CLDN1 mAb treatment inhibits pro-inflammatory and pro-fibrogenic signaling in PSC mouse and patient-derived models

To investigate the mechanism of action of CLDN1 mAb treatment, liver gene expression from the three animal models was analyzed using RNA-seq and compared with the perturbed liver transcriptome of patients with PSC.[16] Gene set-enrichment analysis revealed that 1,101 gene sets which were upregulated in their expression in patients with PSC were downregulated following CLDN1 mAb treatment across all mouse models (Fig. 7A). At the same time, 48 gene sets that were downregulated in patients with PSC showed restored expression across all mouse models (Fig. 7A). CLDN1 mAb treatment robustly suppressed the expression of PSC disease drivers and pathogenic signaling pathways (Fig. 7B). These included NF-κB signaling, T cell receptor and macrophage signaling, TGFβ response, collagen formation as well as Notch and KRAS signaling and epithelial-to-mesenchymal transition. Of note, the suppression of bile acid metabolism in patients with PSC was also restored by CLDN1 mAb treatment. The perturbation of key pro-inflammatory and pro-fibrotic signaling pathways was validated in the BDL mouse model on the protein level using IHC and immunoblotting (Fig. 7C and S9A,B). CLDN1 mAb treatment significantly suppressed NF-kB signaling, as shown by decreased p65-positive area in reactive ductules in the BDL model *in vivo* (Fig. 7C), accompanied by marked reduction of nuclear p65 translocation (Fig. S9A). Moreover, CLDN1 treatment resulted in inhibition of pro-fibrotic SRC, AKT and RAS signaling as shown by decreased phosphorylation of SRC, AKT, and decreased RAS protein expression in immunoblot analyses of mouse liver tissues treated with mAb (Fig. 7C and S9B). Since the majority of these proteins have been shown to bind/interact with CLDN1 in the cell membrane[8,27] and the CLDN1 antibody was not internalized following binding to the cholangiocyte cell membrane (Fig. S10A and B), it is likely the mAb inhibits signaling by

validating the loss of CLDN1 expression in DDC-fed KO mice. (K) Plasma ALT (Mann-Whitney, $p = 0.0039$) and (L) ALP (Mann-Whitney, $p = 0.2799$) levels were decreased in *Alb*.Cre/*Cldn1*$^{fl/fl}$ mice. (M) Cldn1 knockout in liver epithelial cells significantly reduced fibrosis development in the DDC mouse model (Mann-Whitney, $p = 0.0011$). (N) Representative images of Sirius red-stained liver of *Alb*.Cre and *Alb*.Cre/*Cldn1*$^{fl/fl}$ mice. Scale bars: 500 μM * p <0.05; ** p <0.01; *** p <0.001; **** p <0.0001. ALP, alkaline phosphatase; ALT, alanine aminotransferase; CPA, collagen proportionate area; DDC, 3,5-diethoxycarbonyl-1,4-dihydrocollidine; mAb, monoclonal antibody; PSC, primary sclerosing cholangitis. (This figure appears in color on the web.)

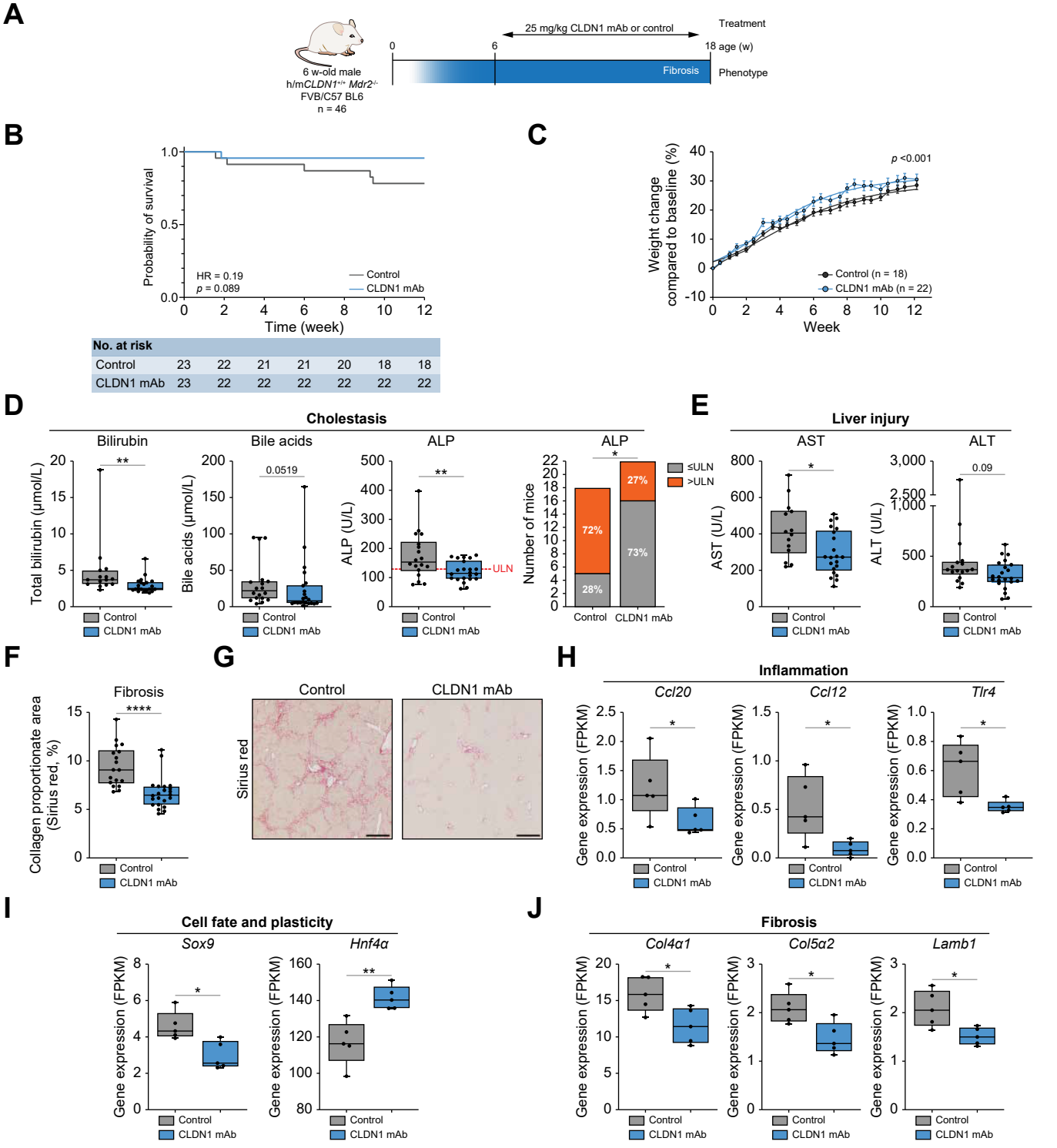

Fig. 6. CLDN1 mAb treatment improves survival, liver function, and liver fibrosis in the *Mdr2*$^{-/-}$ mouse model. (A) Illustration of the experimental approach. (B) Survival analysis of *Mdr2*$^{-/-}$ mice revealing improved survival in CLDN1 mAb-treated group (log-rank test, $p = 0.0887$). (C) Increased growth rate in CLDN1 mAb-treated *Mdr2*$^{-/-}$ mice (extra sum-of-squares F-test, $p < 0.0001$). Error bars: mean ± SEM. (D) CLDN1 mAb treatment significantly decreased markers of cholestasis (bilirubin: $p = 0.0023$; bile acids: $p = 0.0519$, Mann-Whitney, and ALP: $p = 0.077$, *t* test), resulting in the normalization of plasma ALP levels in 73% of mice (Fisher's exact test, $p = 0.01$). (E) Plasma levels of AST (Mann-Whitney, $p = 0.0242$) and ALT (Mann-Whitney, $p = 0.0936$) as markers of liver injury were reduced in CLDN1 mAb-treated group. (F) CLDN1 mAb treatment reduced fibrosis levels as measured by Sirius red CPA (Mann-Whitney, $p < 0.0001$). (G) Representative images of Sirius red-stained livers of control and CLDN1 mAb-treated mice. Scale bars: 500 µm. (H-J) Liver gene expression (RNA-seq, n = 5 *vs.* n = 5) of key inflammation (H), cell fate (I), and fibrosis markers (J). (*Ccl20*: $p = 0.0317$; *Ccl12* $p = 0.0317$; *Tlr4*: $p = 0.0159$; *Sox9*: $p = 0.0159$, *Hnf4a*: $p = 0.0079$; *Col4a1*: $p = 0.0317$; *Col5a2*: $p = 0.0317$; *Lamb1*: $p = 0.0317$, Mann-Whitney). *$p < 0.05$; **$p < 0.01$; ****$p < 0.0001$. Bilirubin (D, left) and AST (E, left) panels show n = 14 control and n = 21 CLDN1 mAb-treated mice. The plasma of four control and one treated mice could not be analyzed due to hemolysis interfering with analyte measurements. ALP, alkaline phosphatase; ALT, alanine aminotransferase; AST, aspartate aminotransferase; CPA, collagen proportionate area; mAb, monoclonal antibody; PSC, primary sclerosing cholangitis. (This figure appears in color on the web.)

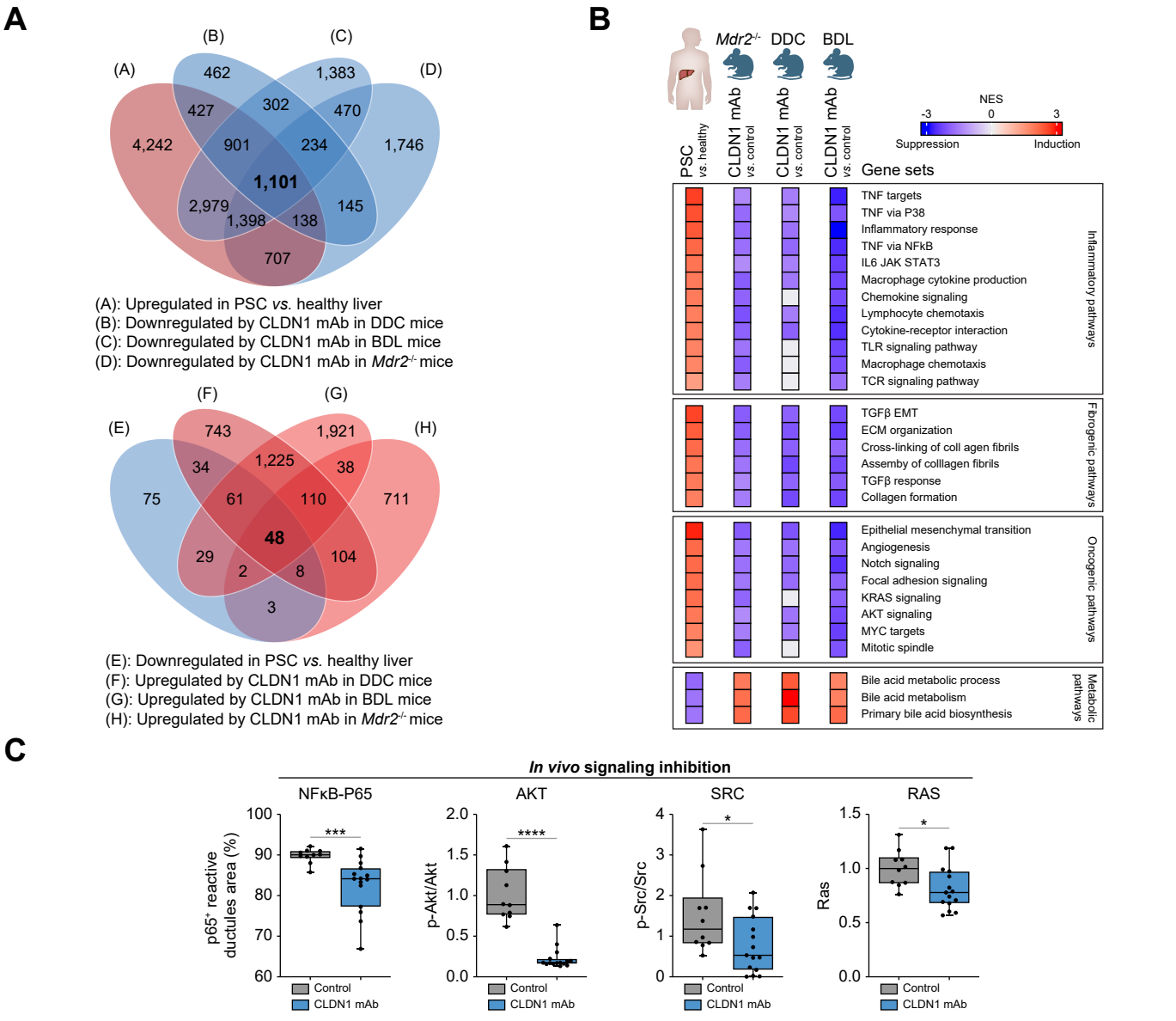

Fig. 7. CLDN1 mAb treatment suppresses pro-inflammatory, pro-fibrotic and pro-carcinogenic signaling pathways *in vivo*. (A) Venn diagrams of pathways differentially enriched in the livers of patients with PSC and in the livers of mouse models. (B) Comparison of PSC liver transcriptome with transcriptomic changes induced by CLDN1 mAb treatment in mouse models. Heatmaps illustrate NES of representative altered gene sets, each condition *vs.* their respective control. (C) Quantification of IHC and immunoblot signals validating transcriptomic findings on the protein level in the BDL mouse model (NF-κB-p65: $p = 0.0004$; AKT: $p < 0.0001$; SRC: $p = 0.0475$; RAS: $p = 0.0226$, Mann-Whitney). * $p < 0.05$; ** $p < 0.01$; *** $p < 0.001$; **** $p < 0.0001$. BDL, bile duct ligation; IHC, immunohistochemistry; mAb, monoclonal antibody; NES, normalized enrichment score; PSC, primary sclerosing cholangitis. (This figure appears in color on the web.)

interfering with protein-protein interactions at the cell membrane.

Liver scRNA-seq analysis of BDL mice revealed additional mechanistic events induced by antibody treatment at single-cell resolution (Fig. 8A). All the major liver cell types were captured, hepatocytes, and macrophages being the most abundant cell types (Fig. S9C). Given the CLDN1 expression profile in scRNA-seq and spatial transcriptomics analyses in patients (Fig. 1, 2), we first focused on epithelial cell biology. CLDN1 mAb treatment induced a significant downregulation of PSC-associated cholangiocyte and hepatocyte marker genes (Fig. 8B). Single-cell gene set variation analysis revealed that CLDN1 mAb treatment reduced the expression of TNFα-NFκB, NOTCH1, AKT, and SRC signaling pathways in both hepatocytes and cholangiocytes (Fig. 8C). The inhibition of pro-inflammatory and pro-fibrogenic signaling was validated on the protein level where CLDN1 mAb treatment modulated SRC, IKBα, and p65 phosphorylation (Fig. S11A and B) in primary human cholangiocytes. The inhibition of epithelial cell signaling resulted in a modulation of macrophage and myofibroblast functions, the effector cell types involved in PSC and biliary fibrosis.[17,28] Single cell-resolved gene expression analysis of the pro-fibrotic niche of the BDL mouse model revealed that CLDN1 mAb treatment suppressed the expression of key pro-inflammatory and pro-fibrotic cytokines in non-parenchymal cells (Fig. 8D), resulting in the suppression of

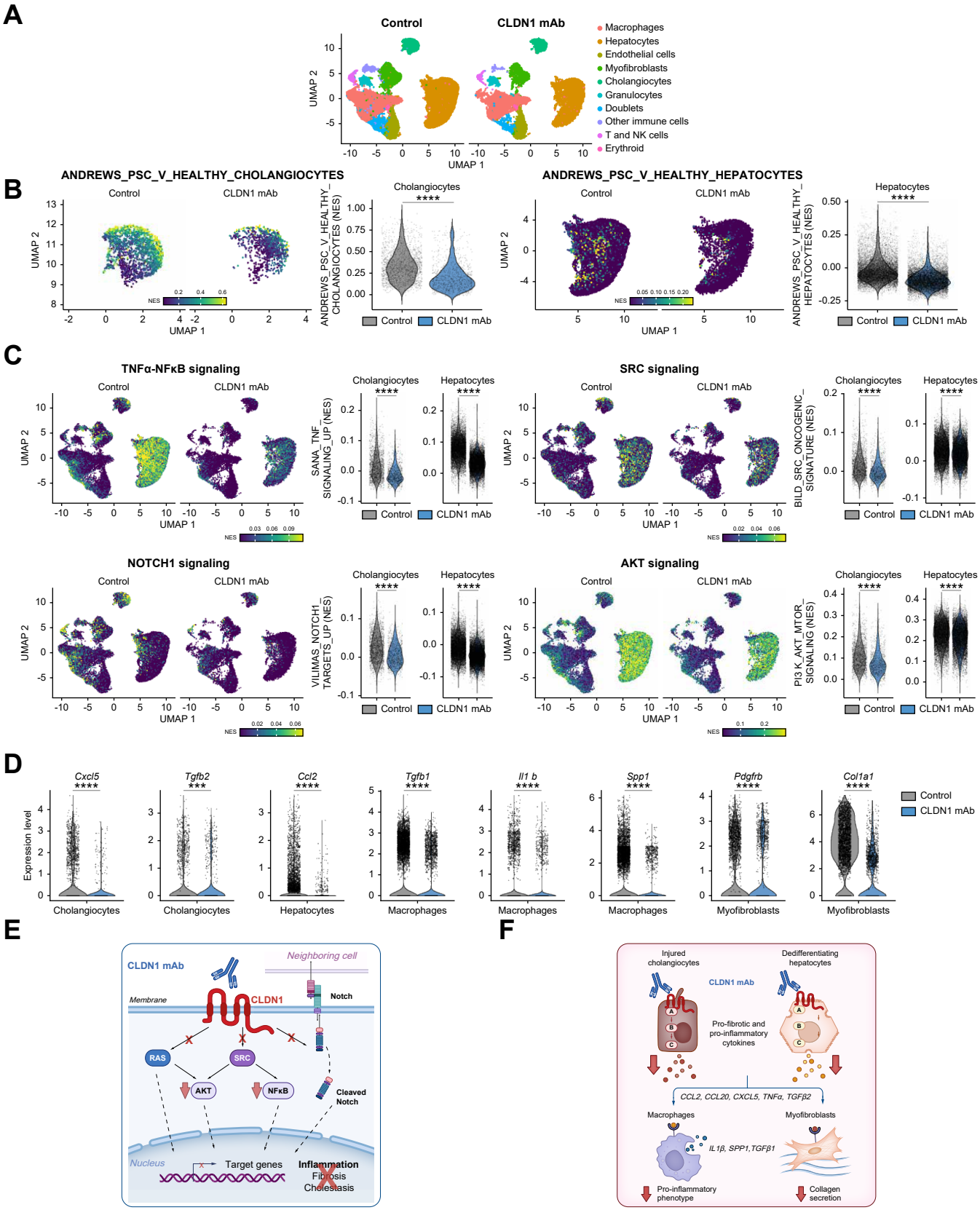

Fig. 8. CLDN1 mAb treatment suppresses pro-inflammatory and pro-fibrotic signaling in liver epithelial cells with inhibition of macrophage and fibroblast activation. (A) scRNA-seq clustering of livers from the BDL mouse model. (B) scGSVA enrichment analysis of gene signatures of PSC cholangiocytes and PSC hepatocytes (Mann-Whitney, both p <0.0001). (C) scGSVA enrichment analysis of TNF–NF-kB, SRC, NOTCH1, and AKT signaling pathways (Mann-Whitney, all p <0.0001). (D) Cell type-specific gene expression of key mediators of the pro-fibrotic niche in biliary fibrosis, showing the ultimate effect of CLDN1 mAb on collagen

the expression of major ECM components in fibroblasts, including *Col1a1* (Fig. 8D).

Collectively, these results identify the targeted cell types and mechanistic events through which CLDN1 mAb treatment improves cholestatic liver disease.

Discussion

In this study, we identify CLDN1 as a previously unrecognized driver and therapeutic target for PSC. This discovery is based on the following key findings: (1) CLDN1 is overexpressed in liver tissues of patients with PSC and its level of expression correlates with disease progression (Fig. 1); (2) CLDN1 expression co-localizes with disease drivers and pathways in the diseased livers of patients with PSC (Figs 2 and 3); (3) a mAb targeting exposed CLDN1 on cholangiocytes and hepatocytes reduces fibrosis, inflammation and cholestasis – hallmarks of PSC – in three state-of-the-art mouse models (Figs 4-6); (4) a loss-of-function study using a liver-specific CLDN1 knockout mouse model supports a functional role of CLDN1 in PSC disease biology (Fig. 5I-N).

Mechanistically, our data are consistent with a model that CLDN1 overexpression in cholangiocytes and hepatocytes induces pro-inflammatory and pro-fibrogenic signaling (Figs 7 and 8E), resulting in the perturbation of epithelial cell fate and induction of the ductular reaction. Subsequent macrophage and fibroblast activation mediates inflammation, cholestasis and fibrosis (Figs 7 and 8F). Since the pathogenic role of the ductular reaction and these signaling pathways have been well described in PSC disease biology,[5,8,29] it is likely that their inhibition mediates the effects of CLDN1 mAb treatment.

Our study has some limitations: first, we cannot exclude the involvement of other CLDN1-related signaling pathways or additional mechanistic events in mediating the effects of CLDN1 mAb. Second, although we used a large panel of complementary model systems for PSC disease biology, these model systems only partially recapitulate the complex pathogenesis of fibrosing cholangiopathies in patients (*e.g.* absence of IBD or intestinal biology). Third, analysis of fibrosis was limited to Sirius red staining and collagen gene expression. Fourth, further studies will be needed to study whether CLDN1 mAb treatment will reduce the development of CCA in PSC-CCA models.

The overexpression of CLDN1 in PSC tissues across several patient cohorts combined with the robust effect of CLDN1 mAb treatment across three state-of-the-art *in vivo* models without detectable adverse events identify CLDN1 as a previously unrecognized therapeutic target in PSC. The correlation of CLDN1 expression with disease biology (Fig. 1) identifies CLDN1 as a candidate biomarker for patient stratification. The modulation of secretory proteins, including TIMP1, metalloproteinases (Figs 4 and 5), and CCL20 – a cytokine associated with PSC[30] and suppressed by antibody treatment in all models (Figs 4–6) – provides opportunities for non-invasive target engagement markers in patients.

Given the absence of approved therapeutic options and the limited success of compounds in clinical development, treatment with CLDN1 mAb could provide a new opportunity to improve the dismal prognosis of patients with PSC.

Interestingly, we observed that the therapeutic effect of CLDN1 treatment on cholestasis, fibrosis and survival was most pronounced in the BDL model, suggesting that BDL best models the pathways targeted by the antibody. Whether this finding has clinical relevance for patients, *e.g.* large duct *vs*. small duct disease or major strictures, remains to be determined.

A clinical challenge in PSC is the high risk of CCA and HCC and the lack of effective surveillance. Since CLDN1 is overexpressed in CCA and HCC and CLDN1 mAbs have been shown to potently inhibit the development and growth of hepatobiliary cancers in patient-derived tumor models,[8,12,31] it is likely that treatment with mAb will also reduce the risk of CCA and HCC, which are key determinants of outcome and survival in patients with PSC. Furthermore, CLDN1 mAbs have been shown to be safe, including in non-human primates[12] and healthy volunteers.[32] Collectively, the results of this study pave the way for clinical development of CLDN1 mAbs as a first-in-class candidate treatment for PSC.

Affiliations

[1]*Inserm U1110, Institute of Translational Medicine and Liver Diseases (ITM), University of Strasbourg, Strasbourg, France;* [2]*Department of Imaging and Pathology, KU Leuven and University Hospitals Leuven, Leuven, Belgium;* [3]*Department of Immunology, University of Toronto, Toronto, Canada;* [4]*Ajmera Transplant Center, University Health Network, Toronto, Canada;* [5]*Donnelly Centre for Cellular and Biomolecular Research, University of Toronto, Toronto, Canada;* [6]*Division of Gastroenterology, Center for Autoimmune Liver Diseases, European Reference Network on Hepatological Diseases (ERN RARE-LIVER), Fondazione IRCCS San Gerardo dei Tintori, Monza, Italy;* [7]*Department of Medicine and Surgery, University of Milano-Bicocca, Milan, Italy;* [8]*Hepatology and Gastroenterology Unit, ASST Grande Ospedale Metropolitano Niguarda, Milan, Italy;* [9]*Department of Hepatobiliary Surgery, Oslo University Hospital and Institute of Clinical Medicine, University of Oslo, Norway;* [10]*Norwegian PSC Research Center (NoPSC), Oslo, Norway;* [11]*KU Leuven Institute for Single Cell Omics (LISCO), KU Leuven, Leuven, Belgium;* [12]*Department of Biochemistry and Molecular Biology, University of Nebraska Medical Center, Omaha, NE, USA;* [13]*Department of Liver and Gastrointestinal Diseases, Biogipuzkoa Health Research Institute – Donostia University Hospital, University of the Basque Country (UPV/EHU), CIBERehd, Ikerbasque, 20014, San Sebastian, Spain;* [14]*Department of Biochemistry and Genetics, School of Sciences, University of Navarra, Pamplona, Spain;* [15]*Alentis Therapeutics, Allschwil, Switzerland;* [16]*Division of Chronic Inflammation and Cancer, German Cancer Research Center Heidelberg, Heidelberg, Germany;* [17]*M3 Research Institute, Medical Faculty Tuebingen (MFT), Tuebingen, Germany;* [18]*IHU Strasbourg, France;* [19]*Gastroenterology and Hepatology Service, Strasbourg University Hospitals, Strasbourg, France;* [20]*Institut Universitaire de France, Paris, France*

Abbreviations

ACTA2, actin alpha 2; ALB, albumin; ALP, alkaline phosphatase; ALT, alanine aminotransferase; AKT, protein kinase B; AST, aspartate aminotransferase; BDL, bile duct ligation; CCA, cholangiocellular carcinoma; CCL20, C–C motif chemokine ligand 20; CK, cytokeratin; CLDN1, claudin-1; Col1a1, collagen type I alpha 1 chain; Col4a1, collagen type IV alpha 1 chain; Col5a2, collagen type V

production by myofibroblasts (Mann-Whitney, all p <0.0001). (E) Mechanistic model of CLDN1 mAb-mediated inhibition of liver and biliary signaling based on transcriptomic and proteomic analyses. (F) Mechanistic model of CLDN1 mAb-mediated anti-fibrotic and anti-inflammatory efficacy in preclinical models for PSC based on scRNA-Seq analyses. *p <0.05; **p <0.01; ***p <0.001; ****p <0.0001. BDL, bile duct ligation; CLDN1, claudin-1; mAb, monoclonal antibody; PSC, primary sclerosing cholangitis; scGSVA, single-cell gene set variation analysis; scRNA-seq, single-cell RNA sequencing. (This figure appears in color on the web.)

alpha 2 chain; CXCL6, C-X-C motif chemokine ligand 6; DDC, 3,5-diethoxycarbonyl-1,4-dihydrocollidine; ECM, extracellular matrix; Epcam, epithelial cell adhesion molecule; FBLN2, fibulin 2; HCC, hepatocellular carcinoma; HNF4A, hepatic nuclear factor 4 alpha; IBD, inflammatory bowel disease; IKBα, inhibitor of NF-κB alpha; KRT7, cytokeratin 7; KRT19, cytokeratin 19; Lamb1, laminin subunit beta 1; MASH, metabolic dysfunction-associated steatohepatitis; MMP7, matrix metallopeptidase 7; MMP9, matrix metallopeptidase 9; NF-κB, nuclear factor kappa B; PSC, primary sclerosing cholangitis; RELA, v-rel avian reticuloendotheliosis viral oncogene homolog A; SPP1, secreted phosphoprotein 1 (osteopontin); SOX4, SRY-box transcription factor 4; Tgfb, transforming growth factor beta; TIMP1, tissue inhibitor of metalloproteinases 1; TNFα, tumor necrosis factor alpha; TNFRSF12A, TNF-related weak inducer of apoptosis receptor.

Financial support

The authors acknowledge the following financial support: European Research Council Grant ERC-AdG-2020 FIBCAN (T.F.B.); ARC Grant TheraHCC2.0 IHUARC, IHU201301187 (T.F.B.); French National Research Agency RHU DELIVER (ANR-21-RHUS-0001) and LABEX ANR-10-LABX-0028_HEPSYS (T.F.B.); the University of Strasbourg Foundation, the Institut Universitaire de France (IUF), Paris, France (TFB), the Alsace Cancer Foundation (T. F. B), the German Research Foundation (DFG) RO 5983/1-1 (N.R.). This work of the Interdisciplinary Thematic Institute IMCBio, as part of the ITI 2021-2028 program of the University of Strasbourg, CNRS and Inserm, was further supported by IdEx Unistra (ANR-10-IDEX-0002), and by SFRI-STRAT'US project (ANR 20-SFRI-0012) and EUR IMCBio (ANR-17-EURE-0023) under the framework of the French Investments for the Future Program and the France 2030 program. JMB was funded by Spanish Carlos III Health Institute (ISCIII) [FIS PI18/01075, PI21/00922 and Miguel Servet Program CPII19/00008 to JMB) co-financed by the European Commission, and the European Union's Horizon 2020 Research and Innovation Program [ESCALON; grant number 825510]. ÆPIC was supported by University of Strasbourg IdEX 2024 "Dispositifs plateformes" (RDGGPJ2403M).

Conflict of interest

Inserm, the University of Strasbourg, the Strasbourg University Hospitals and Alentis Therapeutics have filed a patent application for the use of anti-claudin-1 antibodies to treat cholangiopathies (PCT/IB2023/055666). TFB is founder, shareholder, consultant of Alentis. CS is shareholder of Alentis. GT and RI are employees of Alentis.

Please refer to the accompanying ICMJE disclosure forms for further details.

Authors' contributions

T.F.B. initiated and coordinated the study. F.D.Z. and T.F.B. designed or performed experiments and analyzed data. T.O., O.G., T.R., C.C., M.S., M.C., P.I., F. D.Z. performed CLDN1 expression analyses of human PSC tissues by IHC or immunofluorescence. T.O., G.S., O.G., T.R. performed multiplex iterative labelling by antibody neodeposition (MILAN) studies. F.D.Z., Z.N., M.M., R.D., M.P., A. T.V., L.M. performed animal experiments and analyzed data. E.C. contributed to the design and analyses of cell-based experiments and prepared the libraries for murine scRNA-seq. F.D.Z, F.J., J.M. performed computational analyses on murine tissues. F.D.Z., F.J., J.M., D.N., and S.M. performed computational analyses on PSC patient tissues. T.F., S.Y., and T.H.K. provided liver tissues of the Oslo cohort. M.H.'s laboratory performed IHC staining of mouse liver tissues. J. M.B., N.R., P.D., and C. S. provided important input into the MS. F.D.Z. and T.F. B. designed the figures and wrote the manuscript with edits from all the authors.

Acknowledgements

The authors acknowledge Marine Oudot, Sarah Durand, Cloé Gadenne, Nicolas Brignon, Romain Martin (all Inserm U1110, Strasbourg, France) and Danijela Heide (DKFZ Heidelberg, Germany) for excellent technical assistance, and Prof. A. Kramer (Universitätsspital Zürich) and Palak Trivedi (University of Birmingham) for helpful discussions. The authors acknowledge the Animal Experimentation Platform Infection and Cancer (ÆPIC) (University of Strasbourg, ITM Inserm UMR_S1110, Strasbourg, France) for the management of animal experiments.

Data availability

Transcriptomic data reported in this paper have been deposited at the GEO database with accession numbers GSE261990, GSE261991, and GSE261995.

Supplementary data

Supplementary data to this article can be found online at https://doi.org/10.1016/j.jhep.2025.08.005.

References

Author names in bold designate shared co-first authorship

[1] Vesterhus M, Karlsen TH. Emerging therapies in primary sclerosing cholangitis: pathophysiological basis and clinical opportunities. J Gastroenterol 2020;55:588–614.
[2] Karlsen TH, Folseraas T, Thorburn D, et al. Primary sclerosing cholangitis - a comprehensive review. J Hepatol 2017;67:1298–1323.
[3] Dyson JK, Beuers U, Jones DEJ, et al. Primary sclerosing cholangitis. Lancet 2018;391:2547–2559.
[4] Govaere O, Cockell S, Van Haele M, et al. High-throughput sequencing identifies aetiology-dependent differences in ductular reaction in human chronic liver disease. J Pathol 2019;248:66–76.
[5] Carpino G, Cardinale V, Folseraas T, et al. Hepatic stem/progenitor cell activation differs between primary sclerosing and primary biliary cholangitis. Am J Pathol 2018;188:627–639.
[6] Bowlus CL, Arrivé L, Bergquist A, et al. AASLD practice guidance on primary sclerosing cholangitis and cholangiocarcinoma. Hepatology 2023;77:659–702.
[7] European Association for the Study of the Liver. EASL clinical practice guidelines on sclerosing cholangitis. J Hepatol 2022;77:761–806.
[8] **Roehlen N**, **Saviano A**, El Saghire H, et al. A monoclonal antibody targeting nonjunctional claudin-1 inhibits fibrosis in patient-derived models by modulating cell plasticity. Sci Transl Med 2022;14:eabj4221.
[9] Zeisel MB, Dhawan P, Baumert TF. Tight junction proteins in gastrointestinal and liver disease. Gut 2019;68:547–561.
[10] Nehme Z, Roehlen N, Dhawan P, et al. Tight junction protein signaling and cancer biology. Cells 2023;12:243.
[11] Hasegawa K, Wakino S, Simic P, et al. Renal tubular Sirt1 attenuates diabetic albuminuria by epigenetically suppressing Claudin-1 overexpression in podocytes. Nat Med 2013;19:1496–1504.
[12] Roehlen N, Muller M, Nehme Z, et al. Treatment of HCC with claudin-1-specific antibodies suppresses carcinogenic signaling and reprograms the tumor microenvironment. J Hepatol 2022;(22). 03147–6.
[13] Fofana I, Krieger SE, Grunert F, et al. Monoclonal anti-claudin 1 antibodies prevent hepatitis C virus infection of primary human hepatocytes. Gastroenterology 2010;139:953–964. 964.e1–4.
[14] Mailly L, Xiao F, Lupberger J, et al. Clearance of persistent hepatitis C virus infection in humanized mice using a claudin-1-targeting monoclonal antibody. Nat Biotechnol 2015;33:549–554.
[15] Hadj-Rabia S, Baala L, Vabres P, et al. Claudin-1 gene mutations in neonatal sclerosing cholangitis associated with ichthyosis: a tight junction disease. Gastroenterology 2004;127:1386–1390.
[16] Horvath S, Erhart W, Brosch M, et al. Obesity accelerates epigenetic aging of human liver. Proc Natl Acad Sci U S A 2014;111:15538–15543.
[17] **Andrews TS**, **Nakib D**, Perciani CT, et al. Single-cell and spatial transcriptomics characterisation of the immunological landscape in the healthy and PSC human liver. J Hepatol 2024;(24):3–5.
[18] Colpitts CC, Tawar RG, Mailly L, et al. Humanisation of a claudin-1-specific monoclonal antibody for clinical prevention and cure of HCV infection without escape. Gut 2018;67:736–745.
[19] Mariotti V, Strazzabosco M, Fabris L, et al. Animal models of biliary injury and altered bile acid metabolism. Biochim Biophys Acta Mol Basis Dis 2018;1864:1254–1261.
[20] Mazhar A, Russo MW. Systematic review: non-invasive prognostic tests for primary sclerosing cholangitis. Aliment Pharmacol Ther 2021;53:774–783.
[21] Goet JC, Floreani A, Verhelst X, et al. Validation, clinical utility and limitations of the Amsterdam-Oxford model for primary sclerosing cholangitis. J Hepatol 2019;71:992–999.

[22] **Antoranz A**, **Van Herck Y**, Bolognesi MM, et al. Mapping the immune landscape in metastatic melanoma reveals localized cell-cell interactions that predict immunotherapy response. Cancer Res 2022;82:3275–3290.
[23] Georgiev P, Jochum W, Heinrich S, et al. Characterization of time-related changes after experimental bile duct ligation. Br J Surg 2008;95:646–656.
[24] Fickert P, Stöger U, Fuchsbichler A, et al. A new xenobiotic-induced mouse model of sclerosing cholangitis and biliary fibrosis. Am J Pathol 2007;171:525–536.
[25] Pope JL, Bhat AA, Sharma A, et al. Claudin-1 regulates intestinal epithelial homeostasis through the modulation of Notch-signalling. Gut 2014;63:622–634.
[26] **Popov Y**, **Patsenker E**, Fickert P, et al. Mdr2 (Abcb4)-/- mice spontaneously develop severe biliary fibrosis via massive dysregulation of pro- and antifibrogenic genes. J Hepatol 2005;43:1045–1054.
[27] Kovalski JR, Bhaduri A, Zehnder AM, et al. The functional proximal proteome of oncogenic ras includes mTORC2. Mol Cell 2019;73:830–844.e12.
[28] Lei L, Bruneau A, El Mourabit H, et al. Portal fibroblasts with mesenchymal stem cell features form a reservoir of proliferative myofibroblasts in liver fibrosis. Hepatology 2022;76:1360–1375.
[29] Fiorotto R, Villani A, Kourtidis A, et al. The cystic fibrosis transmembrane conductance regulator controls biliary epithelial inflammation and permeability by regulating Src tyrosine kinase activity. Hepatology 2016;64:2118–2134.
[30] Ellinghaus D, Jostins L, Spain SL, et al. Analysis of five chronic inflammatory diseases identifies 27 new associations and highlights disease-specific patterns at shared loci. Nat Genet 2016;48:510–518.
[31] Muller M, Nehme Z, Roehlen N, et al. Abstract #202 - treatment of cholangiocarcinoma with a humanized anti-Claudin-1 monoclonal antibody. Hepatology 2022;76:S1–S1564.
[32] Alentis Therapeutics. Alentis Therapeutics reports positive topline results from phase 1 multiple ascending dose cohort study. Press release Alentis Therapeutics; 2023. Available at: https://alentis.ch/alentis-therapeutics-reports-positive-topline-results-from-phase-1-multiple-ascending-dose-cohorts-study/ [Accessed September 27, 2023].

Keywords: antibody therapy; biliary fibrosis; cholangiopathies; signaling; proof-of-concept.
Received 13 September 2024; received in revised form 9 July 2025; accepted 5 August 2025; available online 20 August 2025

Journal of Hepatology, Volume *83*

Supplemental information

Claudin-1 is a mediator and therapeutic target in primary sclerosing cholangitis

Fabio Del Zompo, Emilie Crouchet, Tessa Ostyn, Zeina Nehme, Mélissa Messé, Frank Jühling, Romain Désert, Angelica T. Vieira, Julien Moehlin, Diana Nakib, Tallulah Andrews, Catia Perciani, Sai Chung, Gary D. Bader, Ian McGilvray, Chiara Caime, Miki Scaravaglio, Marco Carbone, Pietro Invernizzi, Sheraz Yaqub, Trine Folseraas, Tom H. Karlsen, Gautam Shankar, Mark Primeaux, Punita Dhawan, Jesus M. Banales, Natascha Roehlen, Roberto Iacone, Geoffrey Teixeira, Mathias Heikenwälder, Laurent Mailly, Sonya MacParland, Tania Roskams, Olivier Govaere, Catherine Schuster, and Thomas F. Baumert

Claudin-1 is a mediator and therapeutic target in primary sclerosing cholangitis

Fabio Del Zompo, Emilie Crouchet, Tessa Ostyn, Zeina Nehme, Mélissa Messé, Frank Jühling, Romain Désert, Angelica T. Vieira, Julien Moehlin, Diana Nakib, Tallulah Andrews , Catia Perciani, Sai Chung, Gary D. Bader, Ian McGilvray, Chiara Caime, Miki Scaravaglio, Marco Carbone, Pietro Invernizzi, Sheraz Yaqub, Trine Folseraas, Tom H. Karlsen, Gautam Shankar, Mark Primeaux, Punita Dhawan, Jesus M. Banales, Natascha Roehlen, Roberto Iacone, Geoffrey Teixeira, Mathias Heikenwälder, Laurent Mailly, Sonya MacParland, Tania Roskams, Olivier Govaere, Catherine Schuster, Thomas F. Baumert

Table of contents

Supplementary materials and methods

Animal studies

Animal experiments were performed at Charles River Laboratory (CRL), Lyon (France), at the Inserm U1110 animal facility, Strasbourg (France) according to local laws, ethics committee approval, and authorization by the French Ministry of Research and Higher Education (APAFiS #37313, #41311, #39054, #51912), and in the animal facility of the Department of Biochemistry and Molecular Biology, University of Nebraska Medical Center, Omaha, NE (approved under IACUC #16-058-08-FC). Mice were housed in cages of 3-5 littermates, under 12:12 h dark/light cycles, and allowed *ad libitum* access to food and water. Wild-type C57BL6 or C57BL/6N h/mCLDN1 knock-in (KI) mice engineered to express a human/mouse chimeric CLDN1 were used as indicated. In brief, three human-specific amino acid mutations were introduced into the coding region of the extracellular loop 1 of the mouse CLDN1 gene by Gibson homologous recombination [2]. The resulting transgenic mouse expresses a human/mouse chimeric CLDN1 as a knock-in. The endogenous mouse CLDN1 promoter was not modified to ensure normal expression levels. Human/mouse chimeric CLDN1 mice were bred at Charles River Laboratory (CRL), Lyon.

Liver epithelial-specific CLDN1 knock-out mouse model. Cldn1fl/fl (Cldn1 floxed) (C57BL / 6N-Cldn1tm1c(NCOM)Mfgc / Tcp) mice were re-vitalized from a sperm straw purchased at the Toronto Center for Phenogenomics (TCP) after insemination in female wild type (C57BL / 6J) mice at Charles River Laboratories, Lyon. Albumin (Alb)-Cre (Alb.Cre+) (Stock 003574, B6.Cg-Tg[Alb-cre] 21Mgn/J) mice were purchased from Jackson

Laboratories (Bar Harbor, ME). Cldn1fl/fl mice were bred with Alb.Cre+ mice to generate Cldn1 liver epithelial-specific knockout (Cldn1 KO) mice, with conditional knockout in both hepatocytes and cholangiocytes [3].

3,5-Diethoxycarbonyl-1,4-Dihydrocollidine (DDC) mouse model. 8-to-12 week-old wild-type h/mCLDN1 KI (bred and provided by Charles River Laboratories, France) of male sex or mixed sexes were fed 0.1%-DDC-supplemented diet (SAFE, Augy, France) five days a week for 3 weeks, then for the entire fourth week of study. After the first week, when peribiliary fibrosis was established, mice were randomized into groups receiving weekly i.p. injection of CLDN1-specific mAb (25 mg/kg, n=20), vehicle control (n=20) or an isotype mouse IgG control antibody (25 mg/kg) for 3 weeks (a total of three Ab injections). Mice were sacrificed at the end of week 4, and plasma and livers were harvested for subsequent analyses. Similarly, 8 week-old Alb.Cre and Alb.Cre/Cldn1$^{fl/fl}$ mice were fed with DDC as described above and the liver and blood was harvested at the end of week 4.

Bile duct ligation (BDL) mouse model. The experiment was performed at Charles River Laboratories (Lyon, France) under ethical approval number APAFIS #39054. Forty 8-to-10 week-old h/mCLDN1 KI male mice (bred and provided by Charles River Laboratories, France) underwent surgical ligation of the common bile duct under general anesthesia. After the suture of the abdominal wall, mice were randomized into groups receiving either i.p. injections of CLDN1-specific mAb (25 mg/kg, n=20) or vehicle control (n=20),

repeated on day 4 after surgery (a total of two Ab injections). Mice were sacrificed on day 7 after surgery, and plasma and livers were harvested for subsequent analyses.

Mdr2$^{-/-}$ mouse model. FVB.129P2-Abcb4tm1Bor/J (Jackson Laboratories) mice were crossbred at Charles River Laboratories (Lyon, France) with h/mCLDN1 KI mice to generate double homozygous Mdr2$^{-/-}$ h/mCLDN1 KI mice. The study and sample size were based on previously published experiments using the same mouse model and outcome measure.[4] The design aimed to detect a 20% reduction in the primary endpoint—collagen proportional area (CPA) assessed by Sirius Red staining—with a significance level (α) of 5% and a power (1–β) of 80%. To account for anticipated spontaneous mortality over the course of the study, an additional 30% of mice were included per group. Therefore, forty-six 6-weeks-old Mdr2$^{-/-}$ h/mCLDN1 KI male mice were randomized into groups receiving i.p. injections of CLDN1-specific mAb (25 mg/kg, n=23) or vehicle control (n=23), repeated twice a week for 12 weeks. Mice were sacrificed at the age of 18 weeks, and plasma and livers harvested for subsequent analyses.

Survival analyses in animal models

Kaplan-Meier estimators of animal models survival were compared applying log rank test in GraphPad Prism v9. Confidence intervals of hazard ratios for death in the treatment arm are reported in the graph, along with p-values.

Gut barrier function in vivo assay

DDC treated mice were fasted overnight before performing the assay to minimize fecal matter in the colon. After sedation with Ketamine (100 mg/kg body weight) and Xylazine (10 mg/kg body weight), FITC-dextran (4 kDa; 120 µg/100 µl) [5] was introduced into the colon by rectal administration (using a blunt needle modified for this purpose). After a 30-minute incubation, blood was collected by retro-orbital bleeding in the sedated mice using standard heparinized microhematocrit capillary tubes. Whole blood was centrifuged at 2000 x g for 15 minutes to extract plasma for measurement. Fluorescence was measured using a microplate fluorescence reader at an excitation wavelength of 485 nm and an emission wavelength of 528 nm. The concentration was determined using a standard curve and compared to plasma from untreated mice. Protocol was approved under IACUC # 17-126-11-FC.

Immunohistochemistry staining of patient liver tissues

Manual DAB stainings were performed on formalin-fixed paraffin embedded (FFPE) sections cut at 5 µm from the local biobank of the Department of Imaging and Pathology, KU Leuven (Belgium), the Department of Medicine and Surgery of the University of Milano-Bicocca (Italy), and the Norwegian PSC Research Center of Oslo (Norway), for which written consent was obtained before sampling under study ethics approved by the regional Committees for Medical and Health Research Ethics of Southeast Norway (reference number 2012/286). After dewaxing, antigen epitope retrieval was performed using the EnVision FLEX Target Retrieval Solution Low pH (ref K800521-2) in a PT link instrument (Agilent, ref PT20027). Endogenous peroxidase was blocked for 5 minutes

using the Dako REAL Peroxidase-Blocking Solution (ref S202386-2). Slides were incubated with anti-CLDN1 antibody (1:200, Elabscience, E-AB-30939) for 30 minutes, followed by 30 minutes incubation with an horseradish peroxidase (HRP) labelled secondary antibody. 3.3'-Diaminobenzidine (DAB) chromogen was added for visualization of the staining (10 minutes) and slides were counterstained with hematoxylin, dehydrated and mounted. Images were captured using the Leica DFC290 HD Digital FireWire Camera (Leica Microsystems).

Immunofluorescence staining of patient liver tissues

Fluorescent staining was performed on formalin-fixed paraffin-embedded sections cut at a thickness of 5 µm from the local biobank of the Department of Imaging and Pathology, KU Leuven. After dewaxing, antigen epitope retrieval was performed using the EnVision FLEX Target Retrieval Solution High pH (Agilent) in a PT link instrument (Agilent, ref PT20027). Slides were incubated with primary antibodies anti-CLDN1 (1/600, Elabscience, E-AB-30939), anti-CK19 antibody (1/50, Dako, RCK108), anti-TNFalpha (1/200, Proteintech, 7B8A11), for 2 hours. Subsequently, slides were incubated with Alexa Fluor 488-conjugated goat anti-mouse IgG1 (1/300, Jackson ImmunoResearch, no 115545-205), Alexa Fluor 555-conjugated donkey anti-mouse IgG2b (1/400, ThermoFisher Scientific, A21147) and Alexa Fluor 647-conjugated donkey anti-rabbit (1/400, ThermoFisher Scientific, A 31573) for 1 hour. Slides were mounted with ProLong Gold Antifade Mountant (ThermoFisher Scientific, P36941) and images were taken using the Axioscan.Z1 slide scanner (Zeiss) and processed using ImageJ.

Multiple iterative labelling by antibody neodeposition (MILAN)

A tissue micro-array (TMA) was constructed using human FFPE tissue samples of 3 histologically normal looking liver samples (11 cores) and 7 PSC patients (23 cores) (Table S3). The study protocol followed the ethical principles of the Declaration of Helsinki and approval was obtained from the local Ethics Committee (UZ Leuven reference number S63603). Immunofluorescent multiplexing staining was performed on one single TMA section, cut at 3 µm thickness, according to the previously published MILAN protocol [6,7]. Stainings were performed using a panel of primary antibodies as listed in Table S5 on a BOND RX system (Leica), followed by image acquisition using the Axio scan Z1 slidescanner (Zeiss). The acquired images were registered using *imreg* (https:/github.com/cgohlke/imreg) and autofluorescence subtraction was performed using a baseline scan. *StarDIST* [8] was applied on the DAPI channel for cell segmentation. Topological (X/Y coordinates), morphological (nuclear size) and molecular (Mean Fluorescence Intensity, MFI) features were extracted for each cell and MFIs were normalized with Z-scores per sample. CK19+CK7+ cells were identified as cholangiocytes including ductular reactive cells, CK18+CK7-CK19- cells as hepatocytes, CK18+CK7+CK19- cells as intermediate epithelial cells such as de-differentiating hepatocytes, CD31+ cells as endothelial cells, CD14+ or CD163+ or CD68+ cells as monocytes/macrophages, CD3+ cells as T cells and ASMA+ cells as fibroblasts/smooth muscle cells. UMAP clustering was performed on a subset of 50’001 cells. During further analyses, cholangiocytes and intermediate epithelial cells were grouped together.

Analysis of CLDN1 expressing cells using the PSC scRNAseq atlas

PSC-cholangiocytes were extracted from the PSC scRNAseq atlas[1] and then stratified for *CLDN1* expression tertiles. Marker genes of *CLDN1*^{High} vs *CLDN1*^{Low} (highest vs lowest tertile) were calculated using *FindMarkers* (Wilcoxon Rank-Sum test) in *Seurat*[9], then ranked according to *-log10(p-value)*avg_log2FC*. Pre-ranked GSEA was run on marker genes using *fgsea*[10] against the whole human collection of the Molecular Signatures Database (MSigDB)[11,12]. Adjusted p-values <0.05 were considered statistically significant. Marker genes of PSC vs healthy cholangiocytes and hepatocytes were calculated using *FindMarkers* in *Seurat*[9], then ranked according to -log10(p-value)*sign(avg_log2FC). The first 200 positively enriched genes were included in the genesets renamed ANDREWS_PSC_V_HEALTHY_CHOLANGIOCYTES and ANDREWS_PSC_V_HEALTHY_HEPATOCYTES, respectively.

Mouse liver tissue fibrosis staining and quantification

Fibrosis content was assessed by Sirius Red staining of formalin-fixed paraffin-embedded (FFPE) slices of whole liver lobes. Stained slides were scanned and files processed using ImageJ (National Institutes of Health, Bethesda, USA) or QuPath v0.4 software[13]. Sirius Red-positive areas were quantified by thresholding on the whole portion of liver parenchyma included in the slide. p65-positive ductular structures were segmented from 5 random areas on scanned p65-stained FFPE slices of whole liver lobes. Quantification of positive areas was performed by thresholding DAB-positive signal in the segmented areas, using QuPath v0.4. Cytokeratin-7-positive area was quantified on scanned Ck7-

stained FFPE slices of whole liver lobes. Quantification was performed by thresholding DAB-positive signal on the whole portion of liver parenchyma included in the slide, using QuPath v0.4.

Western blots of mouse liver samples

Murine livers were dissected into small pieces, then lysed with lysis buffer (Triton 1%; NaCl 50 mM; Tris 50 mM pH 7.6; MgCl2 2 mM in ddH2O) supplemented with proteinase inhibitors (Roche) and phosphatase inhibitors (Sigma Phosphatase Cocktail number 2 and 3). Protein quantification was performed using Thermo Scientific BCA Kit. Proteins were loaded in 15-wells gels. Due to the sample size (n=25), samples were distributed across two electrophoretic gels and run at the same time in the same electrophoretic bath. Proteins from each pair of gels were then transferred at the same time onto the same membrane (TransBlot Turbo midi-size LF PVDF, BioRad) using the transblot turbo protocol (BioRad). After blocking with 5% milk in TBS-0.1% Tween for 60 minutes, membranes were cut, washed then incubated with primary antibodies (Table S6) at 4 °C overnight. Membranes were then washed and incubated with appropriate Horseradish Peroxidase conjugated secondary antibodies at room temperature for 60 minutes. After membrane rinsing, protein immunodetection was performed with Clarity ECL Western Blot Substrate (Biorad) in a ChemiDoc MP Imaging System (Biorad). Immunoblot images were analyzed using Image Lab Software v6.1 (Biorad) or ImageJ, normalizing signals based on stain-free images as loading controls.

RNA extraction from mouse liver tissue

Liver cells were lysed in TRIreagent (Molecular Research Center) using GentleMACS Octo Dissociator, and RNA was purified using Direct-zol RNA MiniPrep (Zymo Research) according to the manufacturer's instructions. RNA quantity and quality were assessed using NanoDrop (ThermoScientific). Gene expression profiling was performed using 250-500 ng total RNA. Illumina library preparation, quality control and sequencing were performed at Novogene (Cambridge, UK).

Gene expression and gene set enrichment analyses by RNAseq

Mouse RNA-seq data were mapped to the mouse genome mm39 using HISAT2. Reads were counted with featureCounts, and a differential expression analysis was performed with DESeq2. GSEA was used for unbiased pathway analysis using Molecular Signature Database (MSigDB)[12,14]. Results from GSEA were adjusted for FDR (false-discovery rate). FDR < 0.25 or < 0.05 was considered statistically significant.

Integrative gene expression analyses of liver tissues of PSC patients and mouse models

Differentially expressed genes of liver tissues of patients with PSC versus control[15], CLDN1 mAb-treated versus control BDL mice, CLDN1 mAb-treated versus control DDC mice, and CLDN1 mAb-treated versus control Mdr2$^{-/-}$ mice were calculated using *DESeq2*[16]. Lists of differentially expressed genes were ranked by -log10(p-value) and the sign of fold-change. Pre-ranked GeneSet Enrichment Analysis (GSEA)[11] was then

performed against the gene set collection of MSigDB[12,14] using standard parameters. Normalized enrichment scores (NES) were filtered at a FDR threshold of 0.25[11]. Venn diagrams for overlapping genesets were drawn using the *VennDiagram* package in R.

MAb binding assay

Primary human cholangiocytes were treated with native CLDN1 mAb and isotype CTRL for 2h at 37°C to allow antibody binding on non-junctional CLDN1 at the cell surface. Cells were washed two times with warm PBS and re-incubated in complete medium at 37°C. To investigate antibody binding, cells were harvested before treatment (T0), after 2, 6, 18, 24 and 48h and fixed in paraformaldehyde 4% for 20 min at room temperature. Cells were then washed with PBS pH 7.2, 0.5% bovine serum albumin and 2 mM EDTA and incubated 30 min with APC-Goat anti-human IgG, secondary antibody diluted in PBS/BSA/EDTA buffer 1:1000 at 4°C (# 109-135-098 Jackson ImmunoResearch). Antibodies binding was assessed by flow cytometry using the CytoFLEX cytometer (Beckman Coulter) and analyses were performed with FlowJo Data analysis software (BD Biosciences).

MAb Internalization assay

CLDN1 mAb and isotype control (CTRL) were stained with a pH-sensitive, brightly fluorescing dyes using pHrodo™ Antibody Labeling Kit 505/525 nm (# P36022, Invitrogen™) according to manufacturer's instructions. The pHrodo dyes covalently bind to antibodies and emits fluorescence only in acidic organelles including endosomes and

lysosomes. Primary human cholangiocytes (Human Biliary Epithelial Cells, HBEpiC, ref. P10654; Batch# 21614, Innoprot, Bizkaia, Spain) were treated with CLDN1 mAb pHrodo™ and isotype CTRL pHrodo™ for 2h at 37°C to allow antibody binding on non-junctional CLDN1 at the cell surface. Cells were washed two times with warm PBS and re-incubated in complete medium at 37°C. To investigate antibody internalization, cells were harvested before treatment (T0), after 2, 6, 18, 24 and 48h and fixed in paraformaldehyde 4% for 20min at room temperature. Cells were then washed with PBS pH 7.2, 0.5% bovine serum albumin and 2 mM EDTA (PBS/BSA/EDTA buffer). Free probe was used as positive control. Antibody internalization was assessed by flow cytometry using the CytoFLEX cytometer (Beckman Coulter) and analyses were performed with FlowJo Data analysis software (BD Biosciences).

Gene expression analyses by qPCR of mouse liver tissues

Liver cells were lysed in TRIreagent (Molecular Research Center) using GentleMACS Octo Dissociator, and RNA was purified using Direct-zol RNA MiniPrep (Zymo Research) according to the manufacturer's instructions. RNA quantity and quality were assessed using NanoDrop (ThermoScientific). Subsequently, total RNA was reverse transcribed (H Minus First Strand cDNA synthesis Mix, ThermoScientific) on a Thermocycler (Bio-Rad T100, Bio-Rad, Hercules). Quantitative PCR was performed on the CFX96 Touch Real-Time PCR Detection system with 10 µL reaction volumes containing 5 µL SYBR Green 2x mix (Bio-Rad), 2 µL of RNAse-free water and 250 nM gene specific sense and antisense primers. For qPCR analyses, Prime PCR SYBR Green Assay /Gene

expression were normalized to the housekeeping gene GAPDH using the ΔΔCt method. Primer sequences are reported in Table S7.

scRNAseq analyses of mouse liver tissue

Single cell suspension was generated using Chromium Next GEM RNA Profiling Sample Fixation Kit (PN-1000414). Briefly, 25 mg of flash frozen mouse liver tissues were fixed in a 4% formaldehyde fixative solution in accordance with manufacturer protocols and dissociated using RPMI + 0.2 mg/ml Liberase and gentleMACS™ Octo Dissociator with Heaters (Miltenyi Biotech). Cell concentration was determined using nuclei staining (DAPI) and Countess II FL Automated Cell Counter (Thermo Fisher). Then, $2x10^6$ fixed cells were hybridized with whole transcriptome probe pairs for 20h (Chromium Fixed RNA Kit, Mouse Transcriptome). After washing, cell suspension was loaded into the Chromium iX (10X Genomics) for partitioning (targeted cell recovery = 10,000 per sample) using the Fixed RNA Profiling kit (10X Genomics). Illumina library preparations were performed in accordance with manufacturer protocols. Libraries quality was assessed using Agilent TapeStation and High Sensitivity DNA ScreenTape. Libraries were pooled according to manufacturer recommendation and sequenced at Biomedical Sequencing Facility (BSF) sequencing platform (CeMM, Medical University of Vienna, Austria). Raw expression data were normalized and scaled using *Seurat* [9], then integrated using *harmony*[17], using standard parameters. Clusters were manually assigned to cell identities based on cluster-

specific marker genes calculated using *FindAllMarkers* function in *Seurat*[9]. Single cell-resolved GSEA was performed using *scGSVA* against mouse collections of the Molecular Signatures Database (MSigDB)[14].

Signaling studies in primary human cholangiocytes

$1x10^5$ HIBEpiCs were cultured as per manufacturer's instructions. After overnight incubation, cells were treated with either CLDN1 mAb (10 µg/mL) or control mAb (10 µg/mL) for 72 hours, with antibodies renewed after the first 48 hours. NFκB signaling was induced by treatment with TNFα (10 ng/ml). 60 minutes post incubation with TNFα, cells were harvested for protein extraction and immunoblotting for IKBα (nuclear factor of kappa light polypeptide gene enhancer in B-cells inhibitor) and P-IKBα (phosphorylated nuclear factor of kappa light polypeptide gene enhancer in B-cells inhibitor). 120 minutes post incubation with TNFα, cells were harvested for protein extraction and immunoblotting of p65 and P-p65 (phosphorylated p65). GAPDH staining was used as loading control. SRC signaling was induced by treatment with PMA (1 µM). 120 minutes post incubation with PMA, cells were harvested for protein extraction and immunoblotting for SRC (SRC proto-oncogene) and p-SRC. B-actin staining was used as loading control. Protein signals were then quantified by imaging.

Supplementary figures

Fig. S1

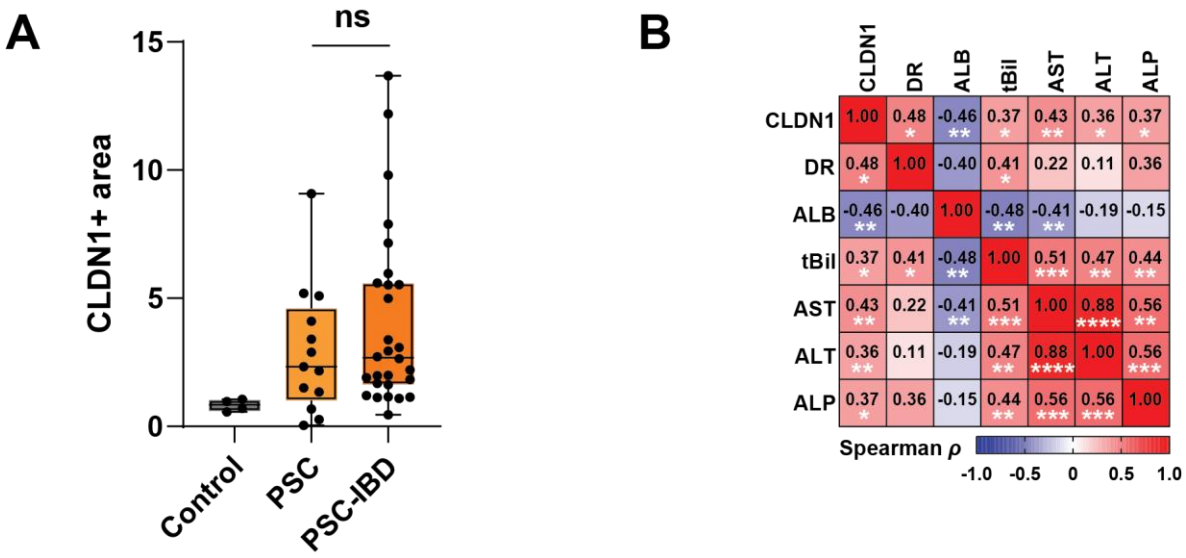

Fig. S1 related to Fig. 1: CLDN1 expression in patient liver samples. (A) CLDN1 expression in the liver of patients with PSC with and without PSC vs healthy controls (Mann-Whitney, p=0.4134). The cohorts are described in Tables S1-2 and CLDN1 expression was analyzed by immunostaining as described in Methods. (B) Correlation of CLDN1 expression in PSC livers with liver function tests, serum albumin levels and the magnitude of the ductular reaction. * p<0.05; ** p<0.01; *** p<0.001; **** p<0.0001.

Fig. S2

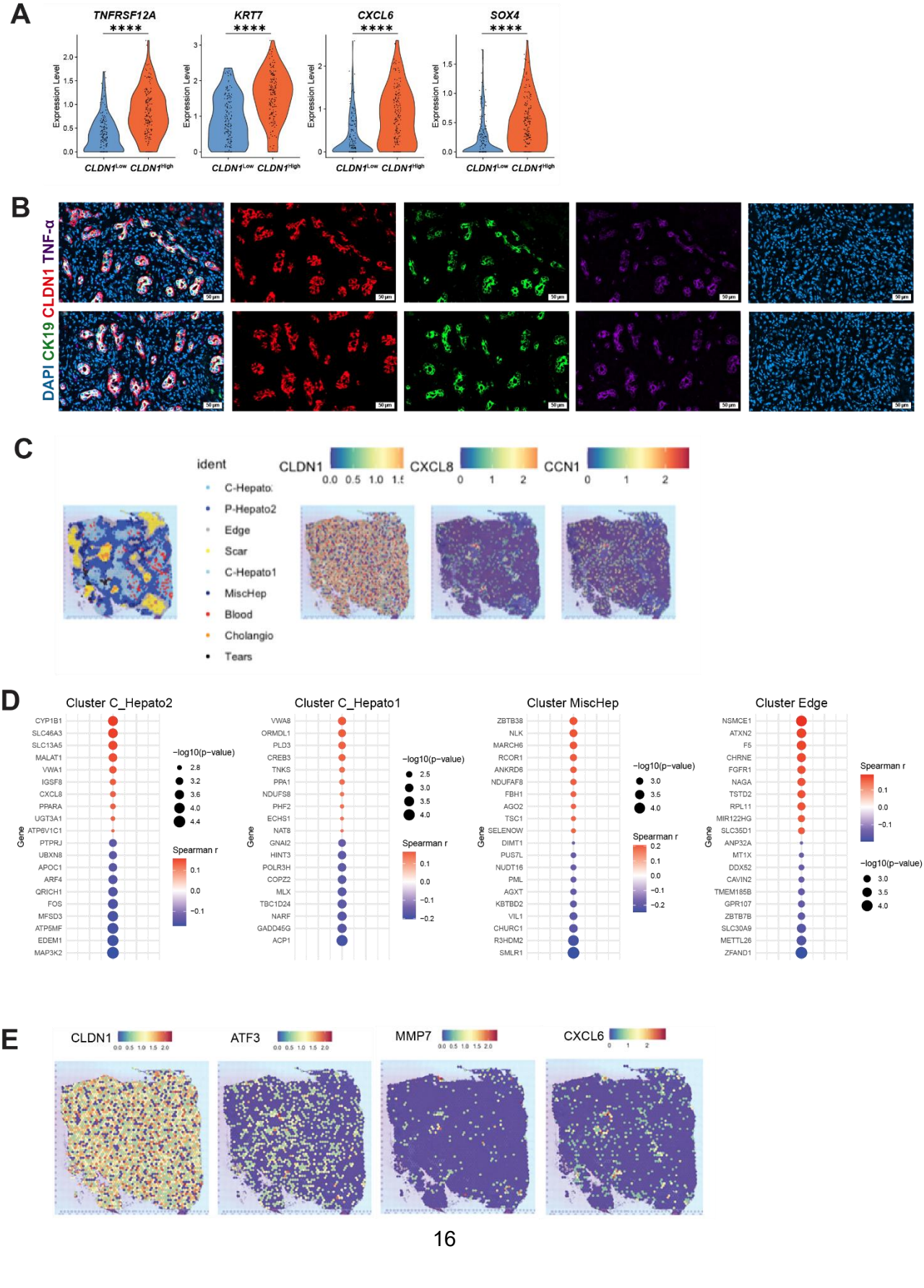
A
TNFRSF12A
KRT7
CXCL6
SOX4
****
Expression Level
CLDN1Low CLDN1High
B
DAPI CK19 CLDN1 TNF-α
C
ident
C-Hepato1
P-Hepato2
Edge
Scar
C-Hepato1
MiscHep
Blood
Cholangio
Tears
CLDN1
CXCL8
CCN1
D
Cluster C_Hepato2
Cluster C_Hepato1
Cluster MiscHep
Cluster Edge
Gene
−log10(p−value)
Spearman r
E
CLDN1
ATF3
MMP7
CXCL6

Fig. S2 related to Fig. 2: CLDN1 expression co-localizes with known PSC disease drivers in patients. (A) Pairwise comparisons of tumor necrosis factor receptor superfamily member 12A (TWEAK Receptor, *TNFRSF12A*), keratin 7 (*KRT7*), C-X-C-motif chemokine ligand 6 (*CXCL6*) and SRY-box transcription factor 4 (*SOX4*) gene expression (Mann-Whitney, all $p<0.0001$), the four most differentially expressed genes in PSC-derived $CLDN1^{High}$ vs $CLDN1^{Low}$ biliary epithelial cells in a scRNAseq atlas of PSC [1]. (B) Triple immunofluorescent staining for CLDN1, CK19 and TNFα of human PSC liver samples. Co-staining showing that CLDN1+ CK19+ ductular cells are major source of TNFα, pro-inflammatory cytokine highly abundant in PSC[34]. Scale bars: 50 μm. (C) Spatial feature plots showing co-localization of CLDN1 expression with *CXCL8* and *CCN1* in PSC. (D) Top 20 genes significantly correlating with CLDN1 expression in the "C_Hepato2", "C_Hepato1" , "MiscHep", and "Edge" clusters of a PSC spatial transcriptomic dataset [1]. (E) Spatial feature plots showing distribution of ATF3, MMP7, and CXCL6 as representative genes highly expressed adjacent to high CLDN1-expressing regions in a spatial transcriptomic dataset [1]. **** $p<0.0001$.

Fig. S3

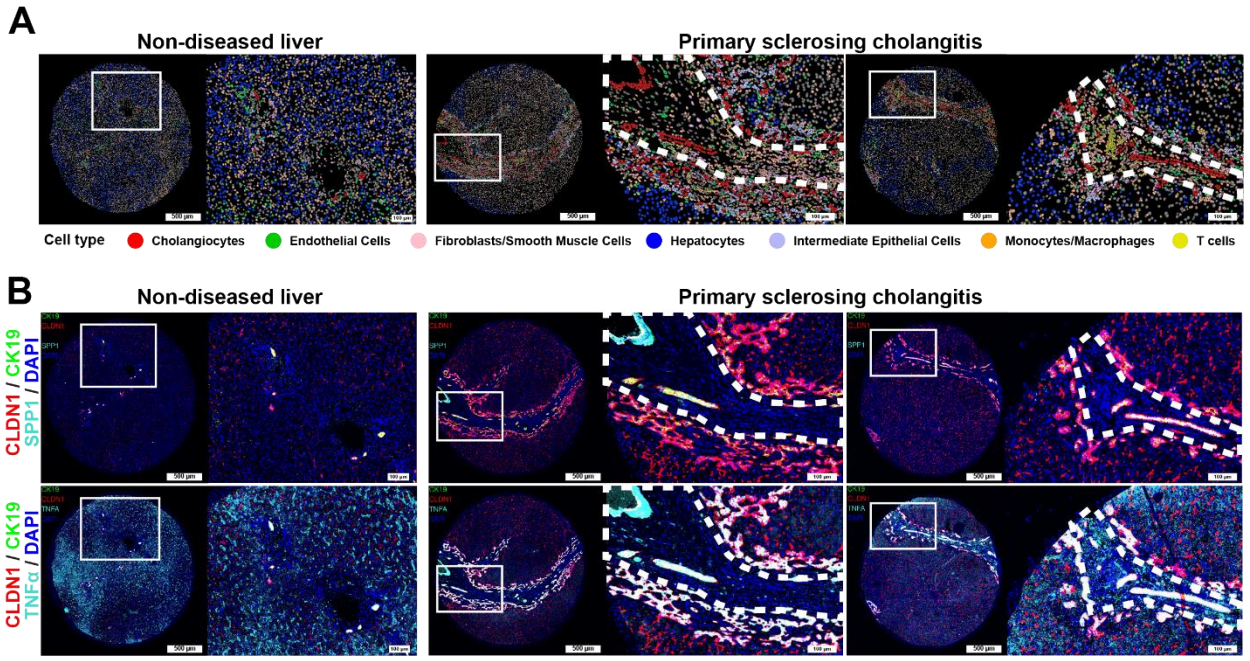

Fig. S3 related to Fig. 3: Spatial proteomics of PSC liver samples. (A) Digital reconstruction of representative TMA cores, phenotyped by spatial proteomics. (B) Composite images of protein expression showing co-staining of CLDN1, CK19, SPP1, DAPI (upper panels), and CLDN1, CK19, TNFα, DAPI (lower panels). Dashed lines mark peri-biliary scars.

Fig. S4

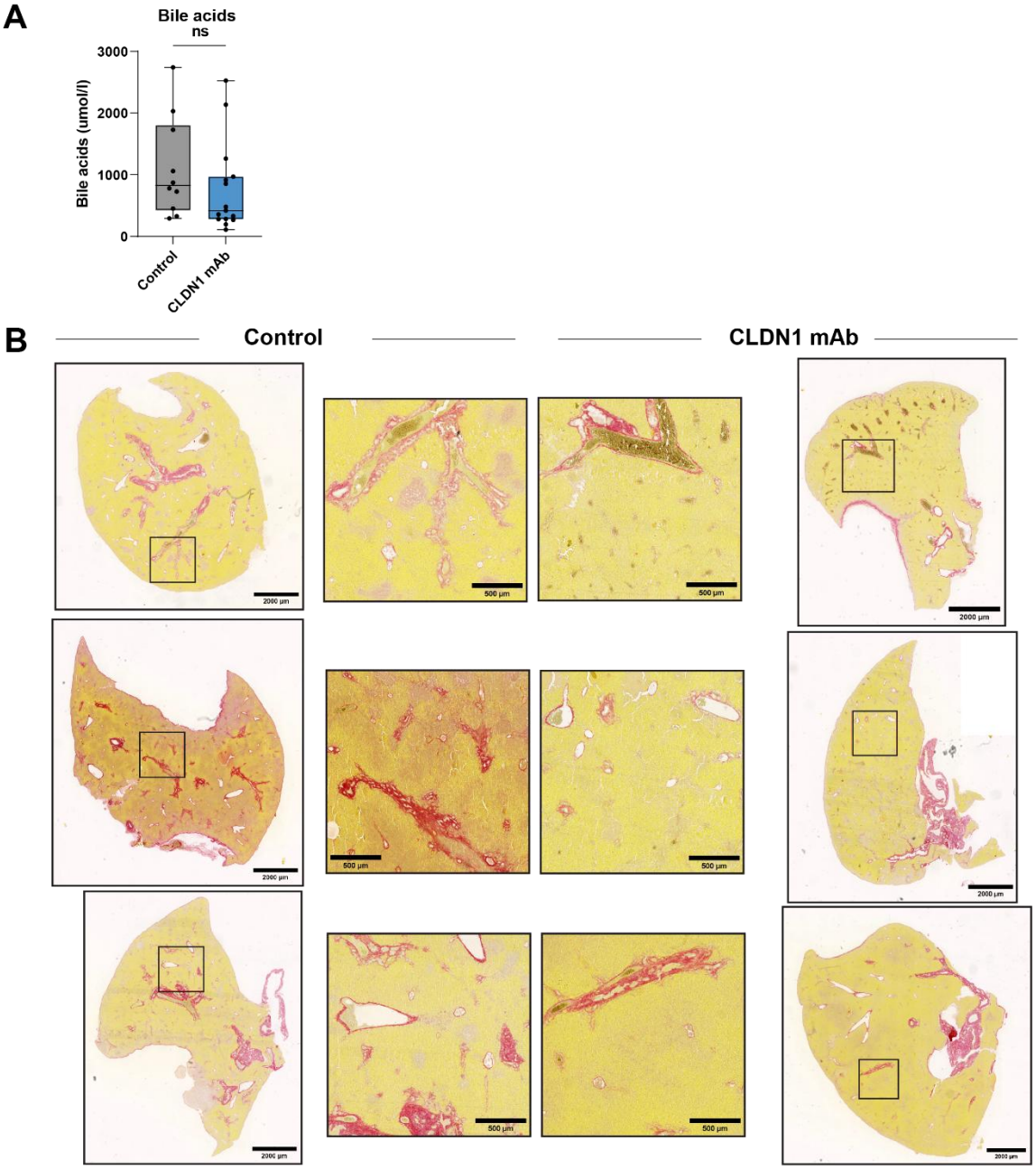
A
Bile acids
ns
Bile acids (umol/l)
3000
2000
1000
0
Control
CLDN1 mAb
B
Control
CLDN1 mAb
2000 µm
500 µm
C
Col1a1
**
Col1a1 fold change
Tgfb1
0.0827
Tgfb1 fold change
Acta2
*
Acta2 fold change
Timp1
**
Timp1 fold change
Control
CLDN1 mAb

Fig. S4 related to Fig. 4: Additional readouts in BDL model CLDN1 mAb treatment study. (A) Plasma bile acid in serum of CLDN1 treated vs control mice shown in Fig. 4 (Mann-Whitney, p=0.1963). (B) Representative samples of Sirius Red-stained CLDN1 mAb-treated and control bile duct-ligated mice shown in Fig. 4. Scale bars: 2000 µm in low-magnification images, 500 µm in high-magnification images. (C) Liver gene expression obtained by qPCR confirmed that CLDN1 mAb treatment reduced the expression of *Col1a1* (Mann-Whitney, p=0.0308), *Tgfb1* (Mann-Whitney, p=0.0827), *Acta2* (Mann-Whitney, p=0.0131), *Timp1* (Mann-Whitney, p=0.0056), and. * p<0.05; ** p<0.01; *** p<0.001; **** p<0.0001; ns: non-significant.

Fig. S5

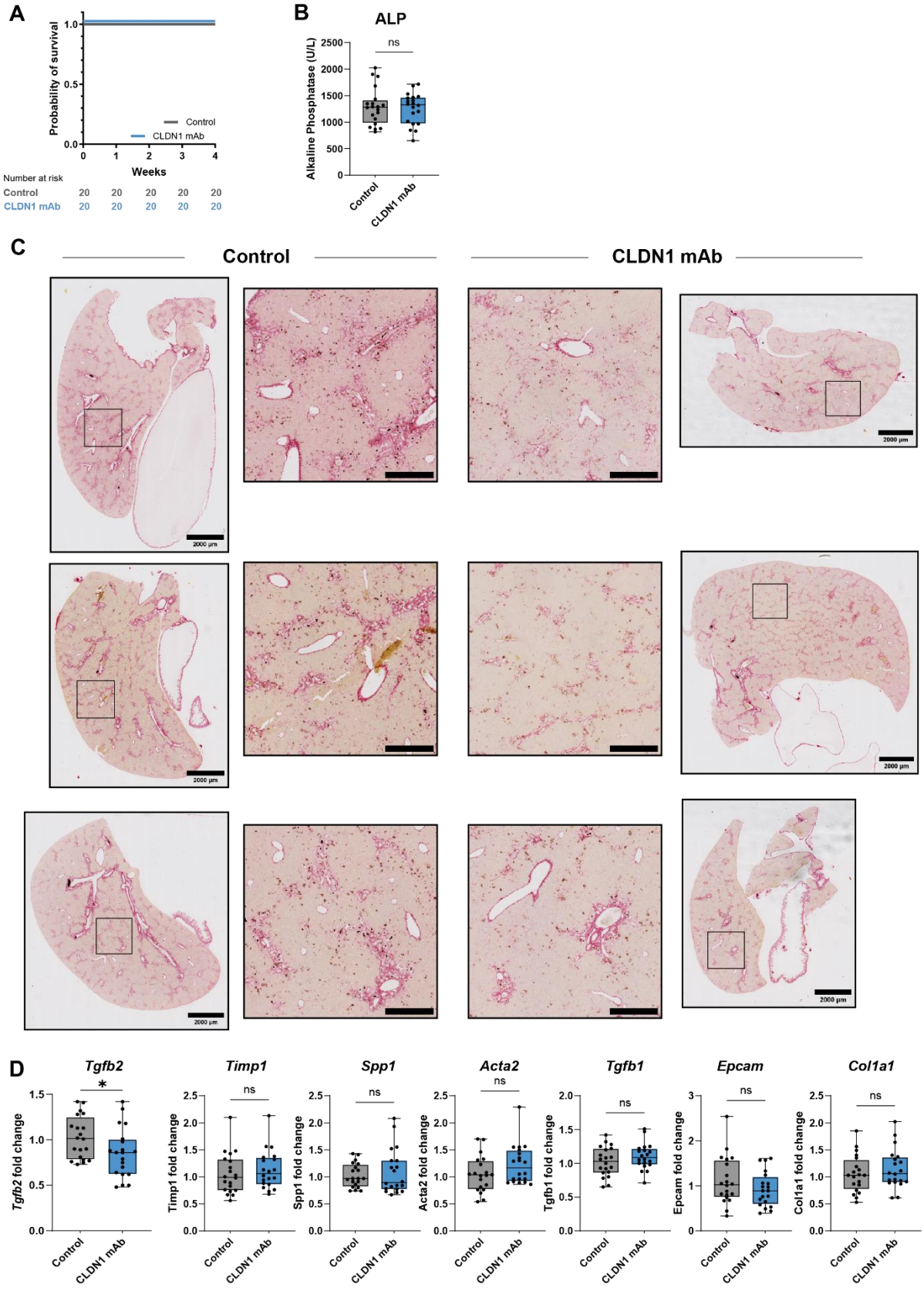
A
Probability of survival
1.0
0.5
0.0
0
1
2
3
4
Weeks
Control
CLDN1 mAb
Number at risk
Control 20 20 20 20 20
CLDN1 mAb 20 20 20 20 20
B
ALP
ns
Alkaline Phosphatase (U/L)
2500
2000
1500
1000
500
0
Control
CLDN1 mAb
C
Control
CLDN1 mAb
2000 μm
D
Tgfb2
*
Timp1
ns
Spp1
ns
Acta2
ns
Tgfb1
ns
Epcam
ns
Col1a1
ns
Tgfb2 fold change
Timp1 fold change
Spp1 fold change
Acta2 fold change
Tgfb1 fold change
Epcam fold change
Col1a1 fold change
Control
CLDN1 mAb

Fig. S5 related to Fig. 5: Additional readouts in DDC model CLDN1 mAb treatment study. (A) Survival analysis of mice shown in the experiment of Fig. 5. (B) Plasma ALP levels of CLDN1-treated and control mice shown in Fig. 5 (Mann-Whitney, p=0.7149). (C) Representative samples of Sirius Red-stained CLDN1 mAb-treated and control bile duct-ligated mice shown in Fig. 5. Scale bars: 2000 µm in low-magnification images, 500 µm in high-magnification images. (D) Liver gene expression for *Tgfb2* (Mann-Whitney, p=0.0368), *Timp1* (Mann-Whitney, p=0.4409), *Spp1* (Mann-Whitney, p=0.7941), *Acta2* (Mann-Whitney, p=0.1472), *Tgfb1* (Mann-Whitney, p=0.2980), *Epcam* (Mann-Whitney, p=0.2618), *Col1a1* (Mann-Whitney, p=0.4570), by means of qPCR. * $p<0.05$; ns: non-significant.

Fig. S6

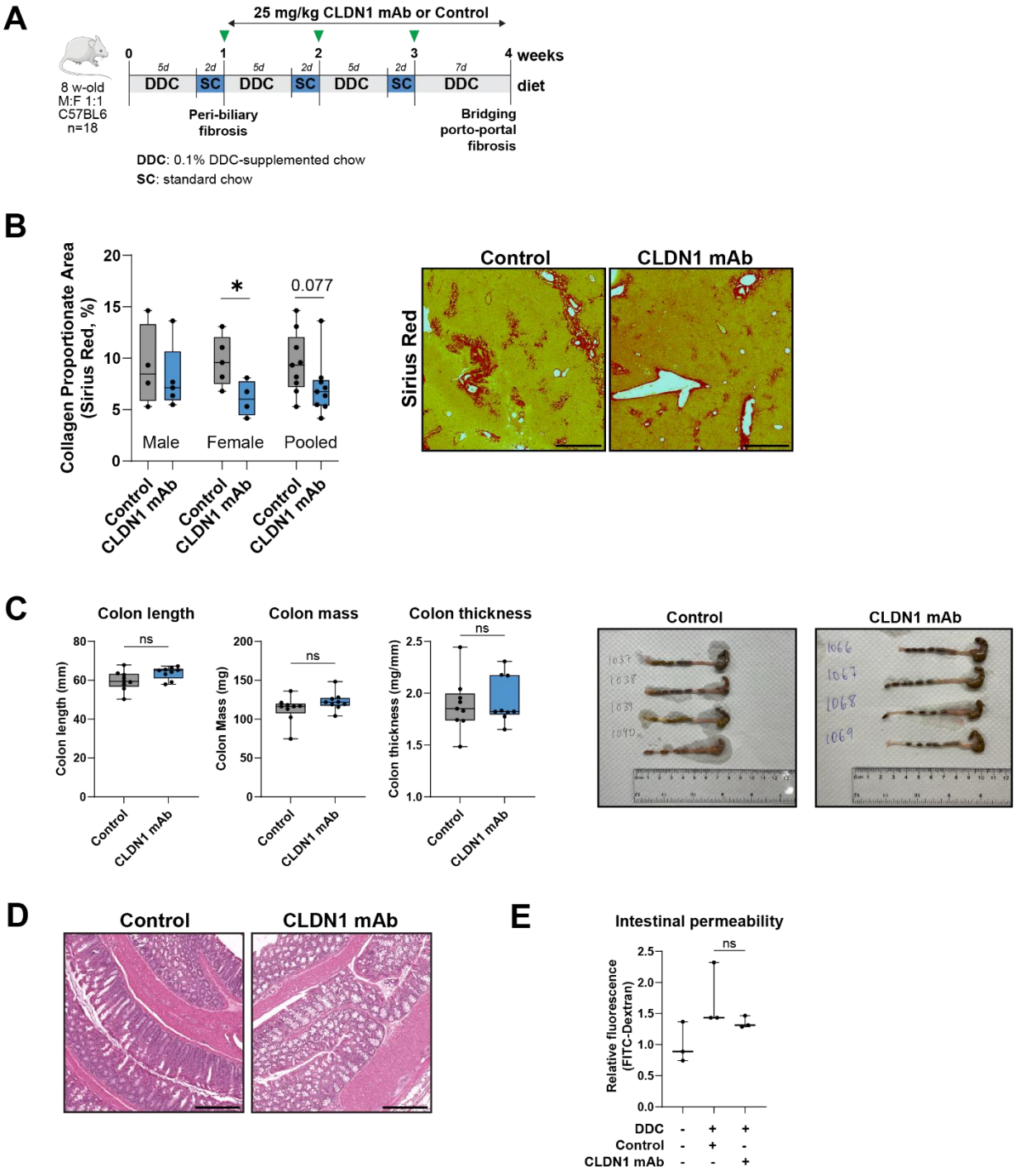

Fig. S6 related to Fig. 5: Absent effect of CLDN1 mAb treatment on colon pathology and intestinal permeability in the DDC mouse model. (A) Experimental design in n=18 wild-type BL6 mice of mixed sexes fed with 0.1% DDC-supplemented diet and treated

with CLDN1 mAb or vehicle control as indicated. (B) Left: Sirius Red Collagen Proportionate Area analysis showing reduction of liver biliary fibrosis in CLDN1 mAb-treated mice, significant in female mice when stratified per animal sex (male mice: p=0.7302; female mice: 0.0317; pooled: p=0.077; Mann-Whitney). Right: representative samples of Sirius Red-stained liver of control and CLDN1 mAb-treated mice. Scale bars: 500 μm. (C) Analysis of macroscopic pathology readouts of mouse colons subjected to DDC diet and treated with CLDN1 mAb or vehicle control. Left to right: colon length (Mann-Whitney, p=0.077), colon mass (Mann-Whitney, p=0.0892), colon thickness (Mann-Whitney, p>0.9999), representative images. (D) Haematoxylin-eosin stained colon of control and CLDN1 mAb-treated mice on 0.1% DDC-supplemented diet, showing no microscopic alterations of pathological significance. Scale bars: 250 μm. (E) Intestinal permeability (Mann-Whitney, p=0.40) as assessed in vivo by FITC-Dextran assay in control and CLDN1 mAb-treated mice on 0.1% DDC-supplemented diet as described in Methods.

Fig. S7

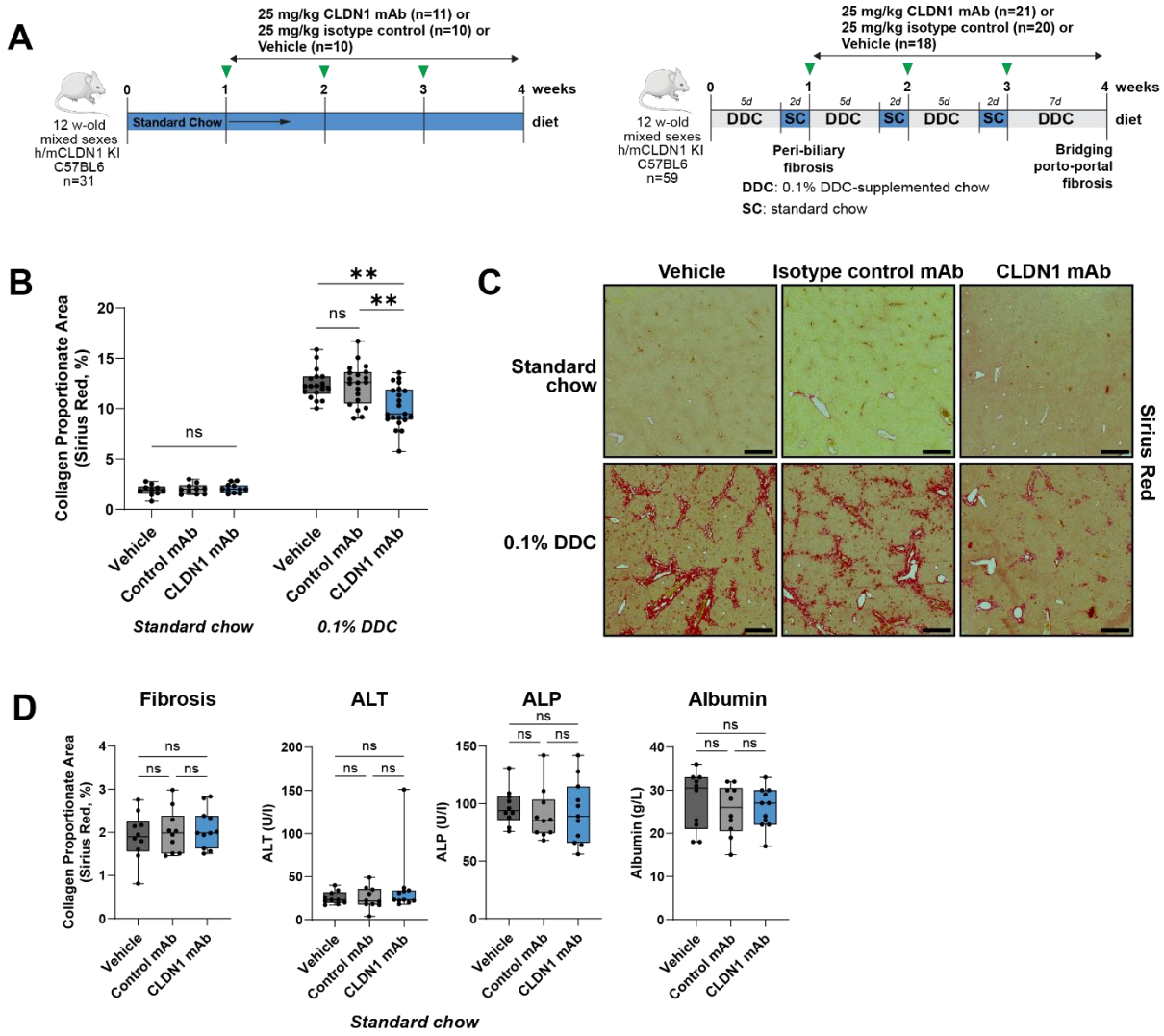

Fig. S7, related to Fig. 5. Effect of CLDN1 treatment on fibrosis in mice with female and mixed sex, validation of the isotype IgG control to show target-specific efficacy in h/mCLDN1 KI mice under DDC and chow diet. (A) Experimental design in n=31 12 w-old, mixed sexes, h/mCLDN1 KI mice fed a standard chow, and n=59 12 w-old, mixed sexes, h/mCLDN1 KI mice fed a 0.1% DDC-supplemented diet. (B) Quantification of Sirius Red Collagen Proportionate Area across all groups, showing no effect of CLDN1 mAb in standard chow-fed mice ($p>0.9999$; Kruskal-Wallis test), confirming reduced biliary fibrosis in CLDN1 mAb-treated mice in the DDC model ($p=0.0077$ vs vehicle;

p=0.0044 vs isotype control mAb; Kruskal-Wallis test) with no detectable effects of isotype control mAb (p>0.9999 vs vehicle; Kruskal-Wallis test). (C) Representative images of Sirius Red-stained liver tissue from all groups. Scale bars: 500 µm. (D) Analyses of vehicle control, isotype control, and CLDN1 mAb effects in h/mCLDN1 KI mice under standard conditions: no differences were detected in regard of Sirius Red Collagen Proportionate Area (all p>0.9999; Kruskal-Wallis test), ALT (p=0.5786; Kruskal-Wallis test), ALP (p=0.4918; Kruskal-Wallis test), albumin (p=0.5442; Kruskal-Wallis test)(left to right). * p<0.05; ** p<0.01; *** p<0.001; **** p<0.0001; ns: non-significant.

Fig. S8

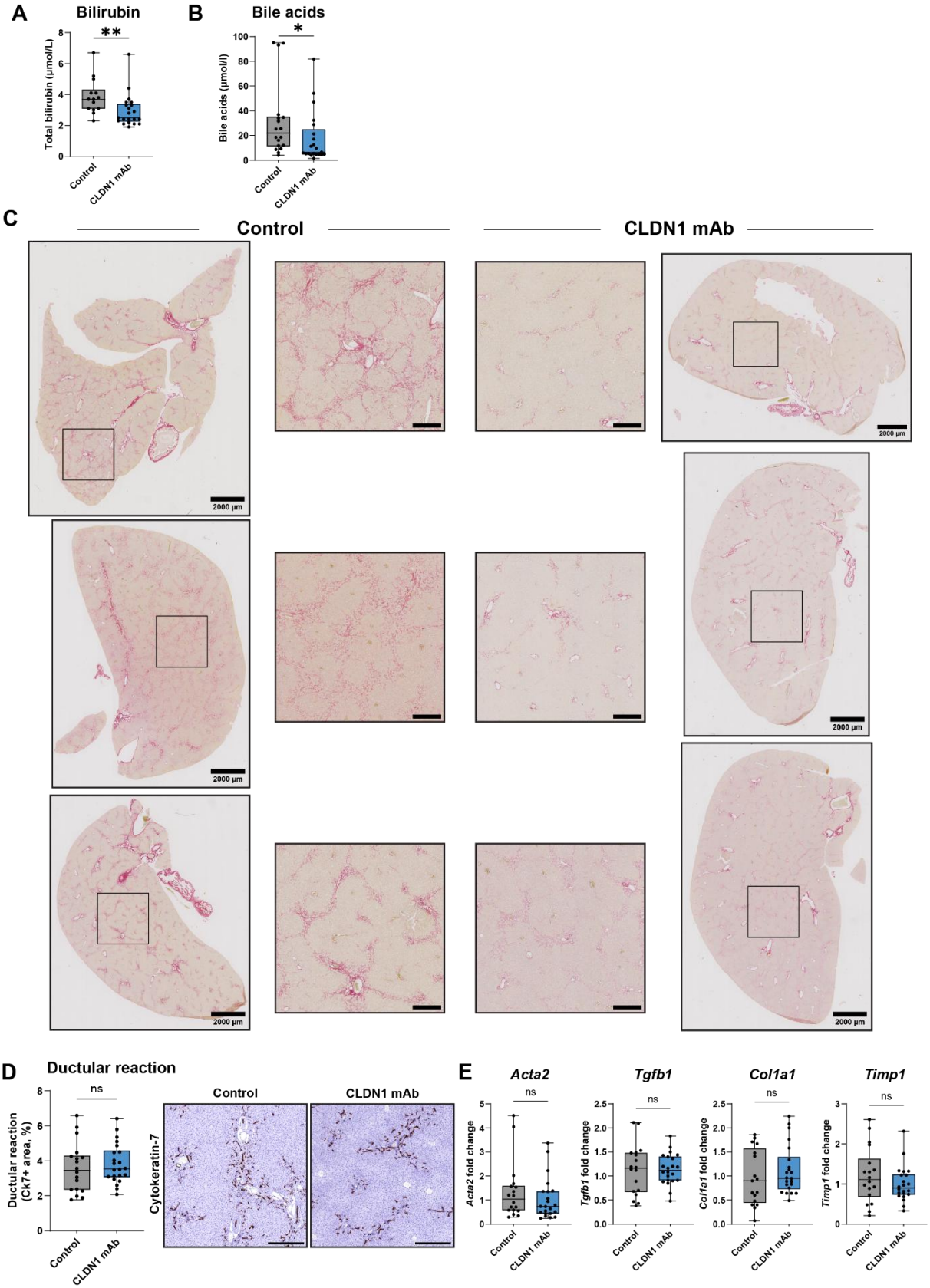
A
Bilirubin
**
Total bilirubin (µmol/L)
Control
CLDN1 mAb
B
Bile acids
*
Bile acids (µmol/l)
Control
CLDN1 mAb
C
Control
CLDN1 mAb
2000 µm
D
Ductular reaction
ns
Ductular reaction (Ck7+ area, %)
Control
CLDN1 mAb
Cytokeratin-7
E
Acta2
Tgfb1
Col1a1
Timp1
ns
fold change

Fig. S8 related to Fig. 6: Additional readouts in *Mdr2*$^{-/-}$ mouse model CLDN1 mAb treatment study. (A) Bilirubin levels in Mdr2$^{-/-}$ mice treated with CLDN1 mAb excluding an outlier from the control group (p=0.0047; Mann-Whitney test). (B) Bile acids levels in Mdr2$^{-/-}$ mice treated with CLDN1 mAb excluding an outlier from the CLDN1 mAb group (p=0.0224; Mann-Whitney test). (C) Representative liver tissue samples of Sirius Red-stained CLDN1 mAb-treated and control bile duct-ligated mice. Scale bars: 2000 µm in low-magnification images, 500 µm in high-magnification images. (D) Quantification of the ductular reaction by cytokeratin-7 immunostaining showed no major differences between CLDN1 mAb-treated and control Mdr2$^{-/-}$ mice (p=0.4427; Mann-Whitney test). Scale bars: 250 µm. (E) Liver gene expression for Acta2 (p=0.3557; Mann-Whitney), Tgfb1 (p=0.8560; Mann-Whitney), Col1a1 (p=0.2949; Mann-Whitney), Timp1 (p=0.3417; Mann-Whitney), analyzed by qPCR. * p<0.05; ** p<0.01; ns: non-significant.

Fig. S9

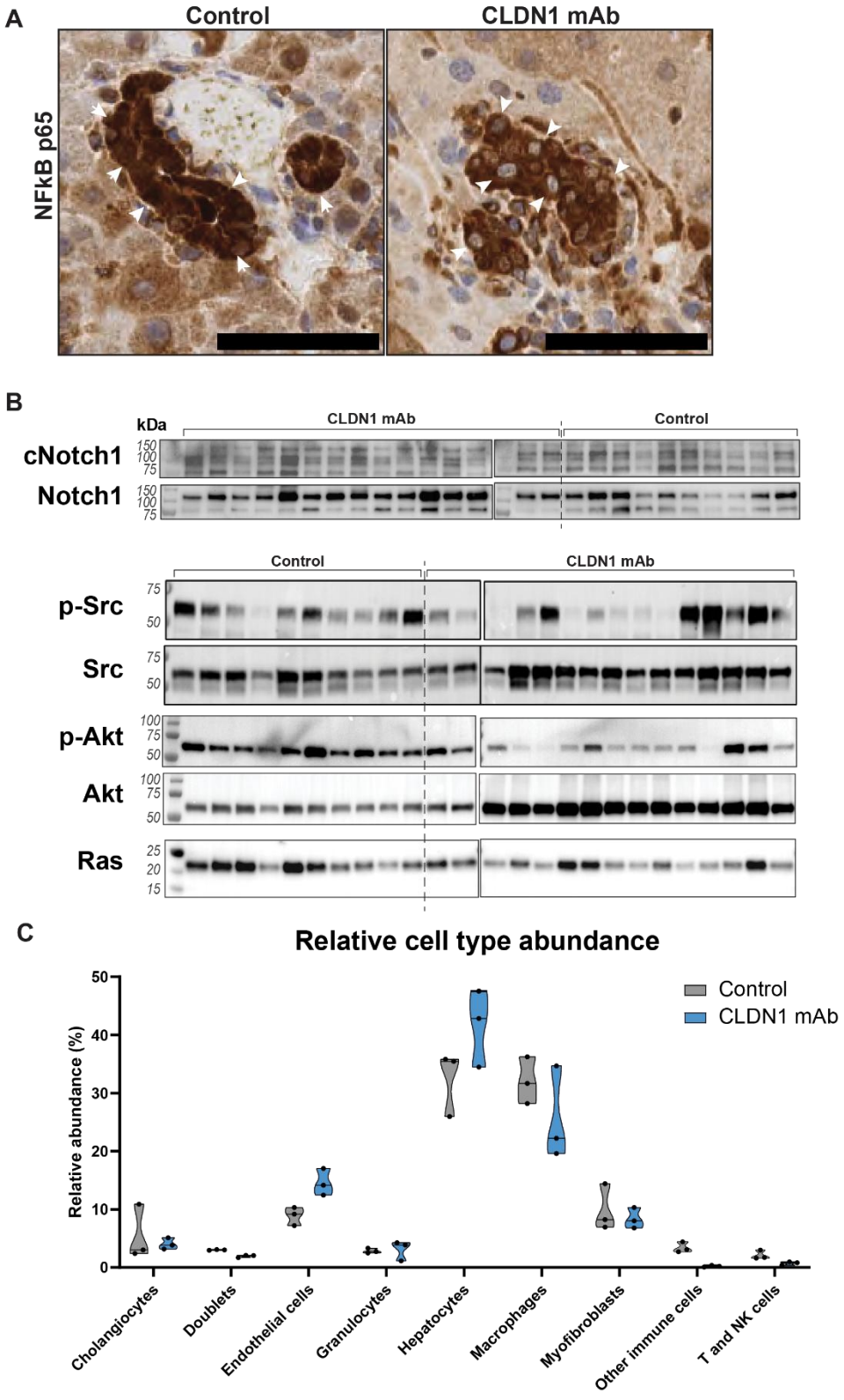
A
Control
CLDN1 mAb
NFkB p65
B
kDa
CLDN1 mAb
Control
cNotch1
Notch1
150
100
75
Control
CLDN1 mAb
p-Src
Src
p-Akt
Akt
Ras
75
50
100
25
20
15
C
Relative cell type abundance
Control
CLDN1 mAb
Relative abundance (%)
50
40
30
20
10
0
Cholangiocytes
Doublets
Endothelial cells
Granulocytes
Hepatocytes
Macrophages
Myofibroblasts
Other immune cells
T and NK cells

Fig. S9, related to Fig. 7: Inhibition of pro-inflammatory and pro-fibrotic signaling by CLDN1 treatment *in vivo* as shown by immunoblot analyses. (A) Representative NFκB-p65 IHC image showing reduced nuclear translocation of P65 in ductular reactive cells of CLDN1 mAb-treated BDL mice. White arrowheads indicate nuclei. Scale bars: 50 μM. (B) Immunoblots of liver protein extracts for p-SRC, SRC, p-AKT, AKT, RAS. (C) Relative cell type abundance of clustered cells analyzed by scRNAseq of the BDL mouse model in CLDN1 treated animals. After scRNAseq cluster annotation, the proportion of cells assigned to each cluster was calculated and plotted for CLDN1 mAb-treated versus control BDL mice.

Fig. S10

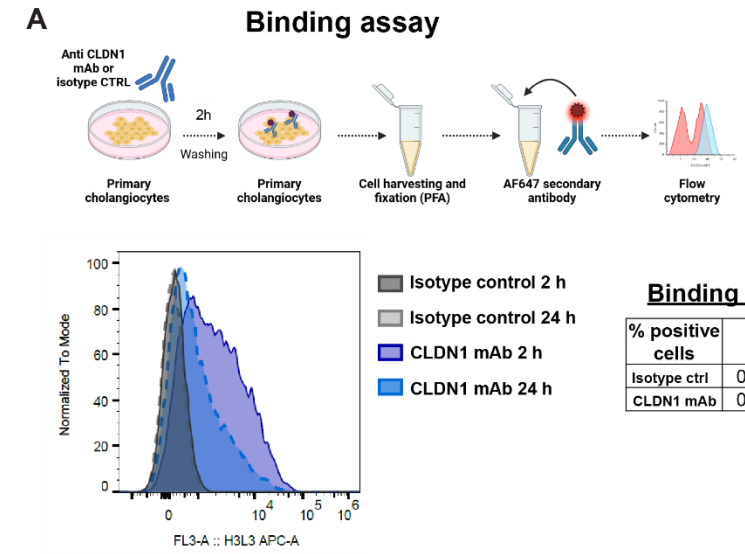

Binding kinetics

% positive cells	0	2h	6h	18h	24h	48h
Isotype ctrl	0,037	1,69	0,2	0,17	0,16	0,015
CLDN1 mAb	0,037	59	34,3	31,1	32,6	20,9

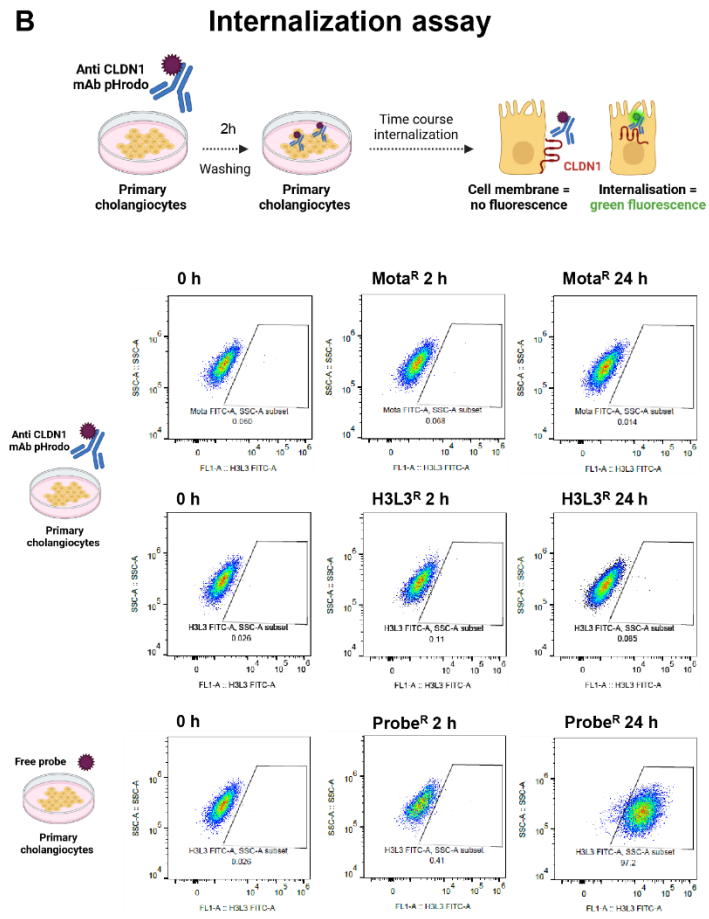

Internalization kinetics

% positive cells	0	2h	6h	18h	24h	48h
Isotype ctrl	0,06	0,068	0,037	0,088	0,014	0,049
CLDN1 mAb	0,026	0,11	0,25	0,16	0,085	0,5
Probe	0,026	0,41	93,9	82	97,2	77,8

Fig. S10, related to Fig. 7: Absent internalization of anti-CLDN1 mAb into primary human cholangiocytes. (A) Flow cytometry-based binding assay of CLDN1-specific

mAb to HIBEpiC primary human cholangiocytes showing robust binding to target cells. (B) Flow cytometry-based internalization assay showing CLDN1 mAb absent internalization in HIBEpiC primary human cholangiocytes. Free probe was used as positive control.

Fig. S11

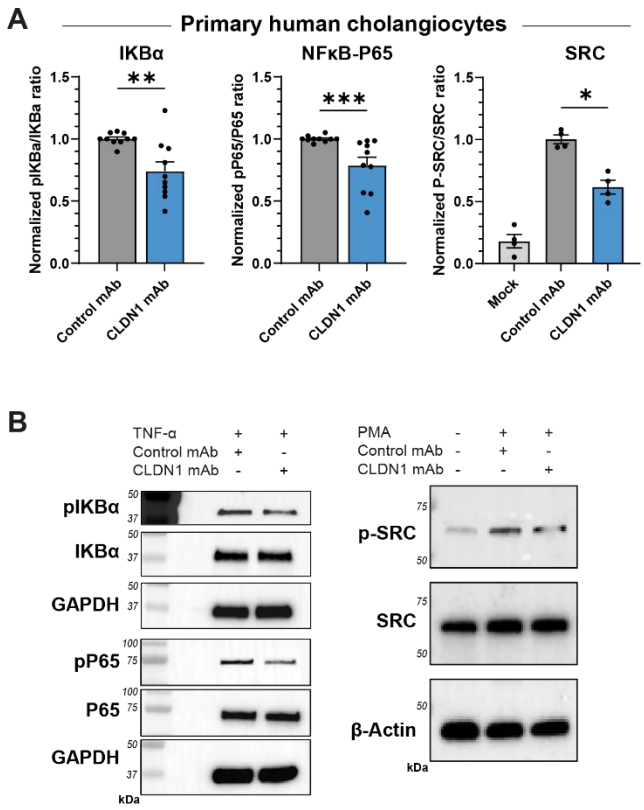

Fig. S11 related to Fig. 7: Immunoblot analyses of NFκB and SRC signaling in primary human cholangiocytes treated with CLDN1 mAb. (A) Quantification of immunoblot signals of IKBα (p=0.0025; Mann-Whitney test), P65 (p=0.0002; Mann-Whitney test), and SRC (p=0.0286; Mann-Whitney test) and their phosphorylated forms in HIBEpiC primary human cholangiocytes. (B) Representative immunoblots of IKBα, P65, and SRC and their phosphorylated forms.

Fig. S12

Full-length blots related to Fig. 7C and Fig. S9B

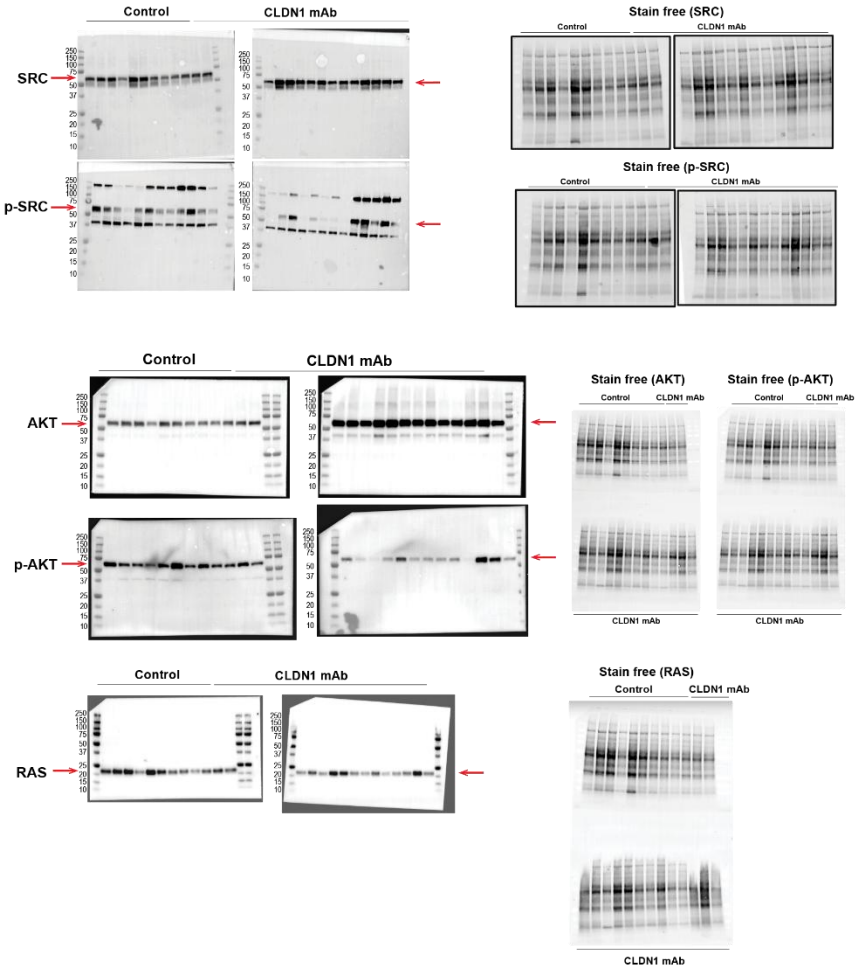

Full-length blots related to Fig. S11 A-B

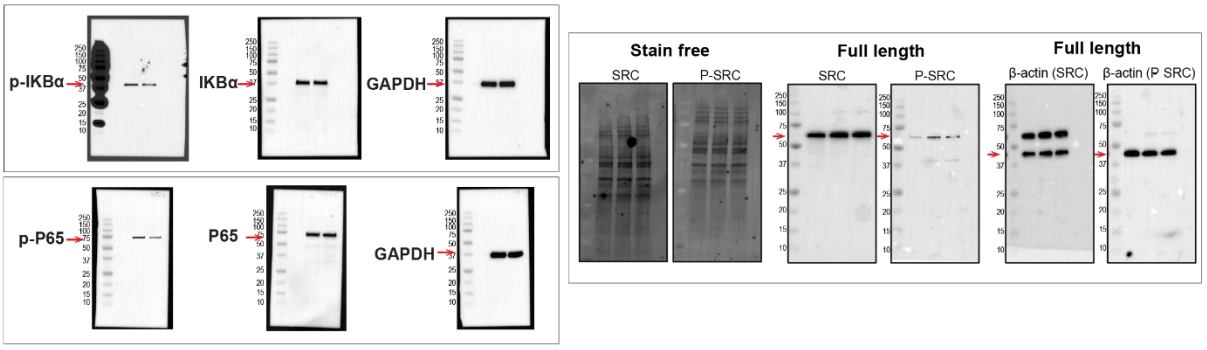

Fig. S12 related to Fig. 7 and Fig. S8: Full-length blots of experiments in Fig. 7 C, Fig. S9 B, and Fig. S11 A-B are shown.

Supplementary tables

Table S1. Clinical features of patients from the Oslo cohort.

Diagnosis	Sex	Age	Stage	Sample type	PSC type	PSC-IBD	ALP	ALP ULN	AST	ALT	tBil	PREsTO (%)					MRS	AOS
												1Y	2Y	3Y	4Y	5Y		
							U/L	U/L	U/L	U/L	µmol/L							
PSC	M	63	Cirrhosis	Explant	LD	UC	419	105	88	76	19	2.6	5	7	11.5	17.4	1	1.87
PSC	M	66	Cirrhosis	Explant	LD	No	392	105	88	97	10	2.3	4.4	6.4	10.3	15.6	0.75	1.71
PSC	F	34	Cirrhosis	Explant	LD	UC	168	105	516	185	218	41.8	65.5	79	92.1	98.1	3.42	3.79
PSC	M	32	Cirrhosis	Explant	PSC-AIH	UC	143	105	67	38	44	1.4	2.7	3.9	6.3	9.6	0.8	2.32
PSC	M	52	Cirrhosis	Explant	LD	UC	n/a	n/a	11	NA	21	0.5	1	1.5	2.4	3.8	n/a	n/a
PSC	M	72	Cirrhosis	Explant	LD	UC	n/a	n/a	111	NA	24	3.6	7	10.1	15.9	23.7	n/a	n/a
PSC	M	30	Cirrhosis	Explant	LD	No	306	105	967	694	164	19.7	35	46.8	64.1	79.8	3.31	n/a
PSC	M	54	Cirrhosis	Explant	LD	UC	80	105	1025	599	262	85.8	97.8	99.6	100	100	5.07	4.5

Diagnosis	Sex	Age	Stage	Sample type	PSC type	PSC-IBD	ALP	ALP ULN	AST	ALT	tBil	PREsTO (%)					MRS	AOS
												1Y	2Y	3Y	4Y	5Y		
							U/L	U/L	U/L	U/L	μmol/L							
PSC	M	41	Cirrhosis	Explant	LD	UC	305	105	150	89	187	50.1	74.4	86.5	96.1	99.4	2.88	3.16
PSC	M	48	Cirrhosis	Explant	LD	UC	164	105	56	58	23	1.2	2.4	3.5	5.5	8.5	2.07	3.37
PSC	M	56	Fibrosis	Explant	LD	UC	134	105	43	84	7	0.4	0.8	1.2	2	3.1	-0.55	1.1
PSC	M	57	Fibrosis	Explant	LD	UC	249	105	59	71	25	1.5	2.9	4.3	6.8	10.4	0.42	1.19
PSC	M	40	Fibrosis	Explant	LD	UC	n/a	n/a	40	NA	10	0.9	1.8	2.6	4.3	6.6	n/a	n/a
PSC	F	61	Fibrosis	Explant	LD	UC	71	105	26	35	7	0.4	0.8	1.2	1.9	3	-0.67	1.18
PSC	M	42	Fibrosis	Explant	LD	UC	255	105	110	119	14	0.7	1.3	1.9	3.1	4.8	0.13	1.27
PSC	M	59	Fibrosis	Explant	LD	UC	122	105	25	23	6	0.4	0.8	1.2	1.9	2.9	-1.01	0.98
PSC	F	43	Fibrosis	Explant	LD	UC	55	105	20	20	5	0.6	1.1	1.6	2.6	4.1	-0.95	0.56
PSC	M	42	Fibrosis	Explant	LD	IC	NA	105	NA	NA	7	0.6	1.1	1.7	2.7	4.2	n/a	n/a

Diagnosis	Sex	Age	Stage	Sample type	PSC type	PSC-IBD	ALP	ALP ULN	AST	ALT	tBil	PREsTO (%)					MRS	AOS
												1Y	2Y	3Y	4Y	5Y		
							U/L	U/L	U/L	U/L	μmol/L							
PSC	F	22	Fibrosis	Explant	LD	No	365	105	113	142	40	4.8	9.2	13.3	20.6	30.3	2.66	3.06
PSC	M	68	Fibrosis	Explant	LD	IC	1045	105	139	95	77	4.5	8.7	12.5	19.5	28.7	2.58	2.4
Healthy liver	M	54	n/a	Resection	n/a	n/a	49	105	42	49	7	n/a	n/a	n/a	n/a	n/a	n/a	n/a
Healthy liver	M	82	n/a	Resection	n/a	n/a	73	105	30	24	12	n/a	n/a	n/a	n/a	n/a	n/a	n/a
Healthy liver	M	65	n/a	Resection	n/a	n/a	97	105	17	18	6	n/a	n/a	n/a	n/a	n/a	n/a	n/a
Healthy liver	F	72	n/a	Resection	n/a	n/a	76	105	10	14	6	n/a	n/a	n/a	n/a	n/a	n/a	n/a

PSC: Primary Sclerosing Cholangitis; M: Male; F: Female; LD: Large-duct PSC; PSC-AIH: PSC with features of autoimmune hepatitis; UC: Ulcerative colitis; IC: Indeterminate colitis; ALP: Alkaline phosphatase; ULN: upper limit of normal; AST: aspartate

aminotransferase; ALT: alanine aminotransferase; tBil: total bilirubin; PREsTO: Primary Sclerosing Cholangitis Risk Estimate Tool; MRS: Mayo Clinic PSC Risk Score; AOS: Amsterdam-Oxford Score; n/a: not available.

Table S2. Clinical features of patients from the Milan cohort.

Diagnosis	Sex	Age	Stage	Sample type	PSC type	PSC-IBD	ALP	ALP ULN	AST	ALT	tBil	PREsTO (%)					MRS	AOS
												1Y	2Y	3Y	4Y	5Y		
							U/L	U/L	U/L	U/L	µmol/L							
PSC	M	22	F0	Biopsy	LD	No	150	115	19	42	32.5	0.5	0.9	1.4	2.2	3.5	-1.28	1.15
PSC	M	29	F0	Biopsy	LD	No	186	115	84	281	8.6	0.4	0.8	1.2	2.0	3.1	-0.66	1.66
PSC	F	45	F1	Biopsy	LD	No	203	104	56	66	10.3	0.4	0.8	1.2	2.0	3.1	-0.47	1.84
PSC	M	41	F1	Biopsy	LD	No	120	116	47	83	20.5	0.8	1.5	2.2	3.5	5.5	0.02	2.04
PSC	M	17	F2	Biopsy	LD	Yes	504	129	128	269	8.6	0.6	1.1	1.6	2.6	4.0	-0.62	1.64
PSC	M	24	F2	Biopsy	PSC-AIH	No	212	129	101	204	13.7	0.5	0.9	1.3	2.1	3.3	-0.87	1.43

Diagnosis	Sex	Age	Stage	Sample type	PSC type	PSC-IBD	ALP	ALP ULN	AST	ALT	tBil	PREsTO (%)					MRS	AOS
												1Y	2Y	3Y	4Y	5Y		
							U/L	U/L	U/L	U/L	μmol/L							
PSC	M	31	F2	Biopsy	LD	Yes	339	115	67	82	8.6	0.8	1.5	2.2	3.6	5.5	-0.38	1.04
PSC	M	32	F2	Biopsy	LD	Yes	121	115	33	48	8.6	0.4	0.7	1.1	1.7	2.7	-1.07	1.3
PSC	F	25	F2	Biopsy	LD	No	483	98	91	103	51.3	1.1	2.2	3.2	5.2	8.0	0.73	1.46
PSC	M	56	F2	Biopsy	LD	Yes	166	129	25	28	18.8	0.5	1.1	1.6	2.5	3.9	-0.59	1.53
PSC	M	47	F2	Biopsy	LD	Yes	846	129	75	93	47.9	3.3	6.4	9.2	14.5	21.7	0.91	2.2
PSC	F	40	F2	Biopsy	LD	Yes	546	98	32	57	112.9	6.6	12.5	17.8	27.3	39.2	0.87	2.84
PSC	M	17	F2	Biopsy	LD	Yes	184	150	185	63	8.6	2.0	3.9	5.7	9.0	13.7	0.76	1.7
PSC	F	53	F2	Biopsy	PSC-AIH	Yes	153	98	55	69	39.3	1.7	3.4	4.9	7.9	12.1	1.23	2.23
PSC	F	27	F2	Biopsy	LD	No	156	98	23	43	13.7	1.0	1.9	2.7	4.4	6.8	-0.66	1.84

Diagnosis	Sex	Age	Stage	Sample type	PSC type	PSC-IBD	ALP	ALP ULN	AST	ALT	tBil	PREsTO (%)					MRS	AOS
												1Y	2Y	3Y	4Y	5Y		
							U/L	U/L	U/L	U/L	μmol/L							
PSC	F	44	F2	Biopsy	LD	Yes	445	116	94	138	13.7	0.6	1.3	1.8	3.0	4.6	-0.57	1.94
PSC	M	49	F2	Biopsy	LD	No	121	116	21	18	18.8	0.5	0.9	1.4	2.2	3.4	-0.14	1.6
PSC	M	46	F2	Biopsy	LD	Yes	409	116	153	296	46.2	3.7	7.2	10.4	16.3	24.3	1.07	2.82
PSC	M	58	F3	Biopsy	PSC-AIH	No	118	129	149	248	34.2	3.1	6.1	8.8	13.9	20.8	1.25	3.05
PSC	F	45	F3	Biopsy	PSC-AIH	No	296	98	112	133	18.8	1.7	3.3	4.7	7.6	11.6	0.98	2.64
PSC	F	62	F3	Biopsy	LD	Yes	205	150	75	82	12.0	0.8	1.5	2.2	3.5	5.4	0.6	2.47

PSC: Primary Sclerosing Cholangitis; M: Male; F: Female; LD: Large-duct PSC; PSC-AIH: PSC with features of autoimmune hepatitis; UC: Ulcerative colitis; IC: Indeterminate colitis; ALP: Alkaline phosphatase; ULN: upper limit of normal; AST: aspartate aminotransferase; ALT: alanine aminotransferase; tBil: total bilirubin; PREsTO: Primary Sclerosing Cholangitis Risk Estimate Tool; MRS: Mayo Clinic PSC Risk Score; AOS: Amsterdam-Oxford Score; n/a: not available.

Table S3. Clinical features of patients from the Leuven cohort.

Diagnosis	Sex	Age	Stage	Sample type
PSC	F	53	F4	Explant
PSC	M	48	F4	Explant
PSC	M	74	F4	Explant
PSC	M	21	F4	Explant
PSC	M	37	F4	Explant
PSC	F	39	F4	Explant
PSC	F	35	F4	Explant
Histologically normal-looking liver tissue adjacent to FNH	F	40	F0	Resection
Histologically normal-looking liver tissue adjacent to FNH	F	37	F0	Resection
Histologically normal-looking liver tissue adjacent to FNH	F	55	F0	Resection

PSC: Primary Sclerosing Cholangitis; M: Male; F: Female; FNH: focal nodular hyperplasia.

Table S4. Quantitative efficacy measures of CLDN1 mAb treatment across mouse models of PSC.

Mouse model	Outcome	Variation (CLDN1 mAb vs Control)	p-value
Bile duct ligation (Fig.4)	Fibrosis	-36.8%	<0.0001
	Survival	0.39 (HR)	0.0800
	ALT	-80.8%	0.0163
	AST	-87.9%	0.0185
	Total bilirubin	-45.2%	0.0118
	Alkaline phosphatase	-34.5%	0.0168
	Bile acids	-49.6%	0.1963
	Albumin	-41.7%	0.0006
DDC (Fig.5)	Fibrosis	-26.1%	<0.0001
	Liver-to-body weight ratio	-9.4%	0.0055
	ALT	-28.6%	0.0009
	Bile acids	-14.5%	0.0559
$Mdr2^{-/-}$ (Fig.6)	Fibrosis	-29.6%	<0.0001
	Survival	0.19 (HR)	0.0887
	Total bilirubin	-32.4%	0.0047
	Bile acids	-70.4%	0.0224
	Alkaline phosphatase	-30.6%	0.0077

	Alkaline phosphatase normalization	2.60 (OR)	0.01
	AST	-32.5%	0.0242
	ALT	-21.5%	0.0936

ALT: Alanine Aminotransferase; AST: Aspartate Aminotransferase; HR: Hazard Ratio; OR: Odds Ratio; DDC: 3,5-Diethoxycarbonyl-1,4-Dihydrocollidine; $Mdr2^{-/-}$: Mdr2 knock-out.

Table S5. Antibodies used in multiple iterative labelling by antibody neodeposition (MILAN).

Target protein	Reference	Clone	Host	Dilution	Manufacturer
CD68	916104	KP1	Mouse IgG1	1/150	Biolegend
SPP1	AF1433	Polyclonal	Goat	1/50	R&D systems
CD163	ab182422	EPR19518	Rabbit	1/50	Abcam
CK19	M0888	RCK108	Mouse IgG1	1/50	Dako
TNFalpha	60291-1-Ig	7B8A11	Mouse IgG2b	1/200	Proteintech
CK7	M7018	OV-TL 12/30	Mouse IgG1	1/50	Dako
CLDN1	E-AB-30939	Polyclonal	Rabbit	1/600	Elabscience
CD3	ab17143	F7.2.38	Mouse IgG1	1/30	Abcam
ASMA	M0851	1A4	Mouse IgG2a	1/100	Dako
CK18	66187-1-Ig	1G11C4	Mouse IgG1	1/300	Proteintech
CD31	LSC-C173974	OTI2C6	Mouse IgG2a	1/250	LSBio
CD14	75181S	D7A2T	Rabbit	1/100	Cell Signaling Technology
AF488-labeled anti-mouse IgG1	115-545-205		Goat	1/300	Jackson ImmunoResearch
AF488-labeled anti-goat	705-545-147		Donkey	1/300	Jackson ImmunoResearch
AF555-labeled anti-mouse IgG2b	A21147		Goat	1/400	Invitrogen
AF555-labeled anti-mouse IgG2a	A21137		Goat	1/400	Invitrogen
AF555-labeled anti-mouse IgG	A31570		Donkey	1/400	Invitrogen
AF647-labeled anti-rabbit	A-31573		Donkey	1/400	Invitrogen

Table S6. Commercial antibodies used in Western blots, IHC, IF.

Protein	Reference	Manufacturer	Use
p65	NB100-2176	Novus Biologicals	IHC
	sc-8008	Santa-Cruz Biotechnology	WB
P-p65	3033S	Cell Signaling Technology	WB
IKBα	4814S	Cell Signaling Technology	WB
P-IKBα	2859S	Cell Signaling Technology	WB
GAPDH	ab9485	Abcam	WB
CLDN1	E-AB-30939	Elabscience	IHC, IF
CK7	ab181598	Abcam	IHC
AKT	4691S	Cell Signaling Technology	WB
p-AKT	9271S	Cell Signaling Technology	WB
SRC	2108S	Cell Signaling Technology	WB
p-SRC	2101S	Cell Signaling Technology	WB
RAS	MA1-012	Invitrogen	WB
CK19	M0888	Dako	IF
TNF-alpha	60291-1-IG	Proteintech	IF
AF488 anti-mouse IgG1	115545-205	Jackson ImmunoResearch	IF
AF555 anti-mouse IgG2b	A21147	ThermoFisher Scientific	IF
AF647- donkey anti-rabbit	A31573	ThermoFisher Scientific	IF

Table S7. qPCR primers used in SYBR Green qPCRs in mice.

Gene	Forward (5'-3')	Reverse (5'-3')
Krt19	CAGGTCAGTGTGGAGGTGGATTC	TCAGCTCCTCAATCCGAGCAAG
Spp1	CCCGGTGAAAGTGACTGATT	GAGATTCTGCTTCTGAGATGGG
Epcam	CAGTGTACTTCCTATGGTACACAGAATACT	CTAGGCATTAAGCTCTCTGTGGATCTCACC
Tgfb2	GCAGATCCTGAGCAAGCTG	GTAGGGTCTGTAGAAAGTGG
Col1a1	AAAGGTGATGCTGGTCCTCC	CATTTCCAGAGGGACCAGGG
Timp1	CCAGAACCGCAGTGAAGAGT	ACAGGGAAACACTGTGCACA
Acta2	GGCATCATCACCAACTGGGA	CACATAXATGGCGGGGACAT
Tgfb1	GTCACTGGAGTTGTACGGCA	TCATGTCATGGATGGTGCCC
Gapdh	TTCACCACCATGGAGAAGGC	TAAGCAHTTGGTGGTGCAGG

Supplementary references

[1] Andrews TS, Nakib D, Perciani CT, et al. Single-cell and spatial transcriptomics characterisation of the immunological landscape in the healthy and PSC human liver. J Hepatol 2024:S0168-8278(24)00003–5.

[2] Avilan L. Assembling Multiple Fragments: The Gibson Assembly. Methods Mol Biol 2023;2633:45–53.

[3] Desert R, Ge X, Song Z, et al. Role of Hepatocyte-Derived Osteopontin in Liver Carcinogenesis. Hepatol Commun 2022;6:692–709.

[4] Fuchs CD, Sroda N, Scharnagl H, et al. Non-steroidal FXR agonist cilofexor improves cholestatic liver injury in the Mdr2-/- mouse model of sclerosing cholangitis. JHEP Rep 2023;5:100874.

[5] Ahmad R, Rah B, Bastola D, et al. Obesity-induces Organ and Tissue Specific Tight Junction Restructuring and Barrier Deregulation by Claudin Switching. Sci Rep 2017;7:5125.

[6] Bolognesi MM, Manzoni M, Scalia CR, et al. Multiplex Staining by Sequential Immunostaining and Antibody Removal on Routine Tissue Sections. J Histochem Cytochem 2017;65:431–444.

[7] Antoranz A, Van Herck Y, Bolognesi MM, et al. Mapping the Immune Landscape in Metastatic Melanoma Reveals Localized Cell-Cell Interactions That Predict Immunotherapy Response. Cancer Res 2022;82:3275–3290.

[8] Schmidt U, Weigert M, Broaddus C, et al. Cell Detection with Star-convex Polygons. In: Vol 11071.; 2018:265–273. Available at: http://arxiv.org/abs/1806.03535 [Accessed August 22, 2024].

[9] Hao Y, Stuart T, Kowalski MH, et al. Dictionary learning for integrative, multimodal and scalable single-cell analysis. Nat Biotechnol 2024;42:293–304.

[10] Korotkevich G, Sukhov V, Budin N, et al. Fast gene set enrichment analysis. 2021:060012. Available at: https://www.biorxiv.org/content/10.1101/060012v3 [Accessed August 11, 2024].

[11] Subramanian A, Tamayo P, Mootha VK, et al. Gene set enrichment analysis: a knowledge-based approach for interpreting genome-wide expression profiles. Proc Natl Acad Sci U S A 2005;102:15545–15550.

[12] Liberzon A, Subramanian A, Pinchback R, et al. Molecular signatures database (MSigDB) 3.0. Bioinformatics 2011;27:1739–1740.

[13] Bankhead P, Loughrey MB, Fernández JA, et al. QuPath: Open source software for digital pathology image analysis. Sci Rep 2017;7:16878.

[14] Castanza AS, Recla JM, Eby D, et al. Extending support for mouse data in the Molecular Signatures Database (MSigDB). Nat Methods 2023;20:1619–1620.

[15] Horvath S, Erhart W, Brosch M, et al. Obesity accelerates epigenetic aging of human liver. Proc Natl Acad Sci U S A 2014;111:15538–15543.

[16] Love MI, Huber W, Anders S. Moderated estimation of fold change and dispersion for RNA-seq data with DESeq2. Genome Biol 2014;15:550.

[17] Korsunsky I, Millard N, Fan J, et al. Fast, sensitive and accurate integration of single-cell data with Harmony. Nat Methods 2019;16:1289–1296.